Complex Fluids and Hydraulic Fracturing

Alexander C. Barbati,[1] Jean Desroches,[2] Agathe Robisson,[3] and Gareth H. McKinley[1]

[1]Hatsopoulos Microfluids Laboratory, Department of Mechanical Engineering, Massachusetts Institute of Technology, Cambridge, Massachusetts 02139; email: gareth@mit.edu

[2]Schlumberger, Paris la Défense 92936, France

[3]Schlumberger-Doll Research, Cambridge, Massachusetts 02139

Annu. Rev. Chem. Biomol. Eng. 2016. 7:415–53

First published online as a Review in Advance on April 6, 2016

The *Annual Review of Chemical and Biomolecular Engineering* is online at chembioeng.annualreviews.org

This article's doi: 10.1146/annurev-chembioeng-080615-033630

Keywords

hydraulic fracturing, porous media, rheology, complex fluids, suspension mechanics, particulate transport

Abstract

Nearly 70 years old, hydraulic fracturing is a core technique for stimulating hydrocarbon production in a majority of oil and gas reservoirs. Complex fluids are implemented in nearly every step of the fracturing process, most significantly to generate and sustain fractures and transport and distribute proppant particles during and following fluid injection. An extremely wide range of complex fluids are used: naturally occurring polysaccharide and synthetic polymer solutions, aqueous physical and chemical gels, organic gels, micellar surfactant solutions, emulsions, and foams. These fluids are loaded over a wide range of concentrations with particles of varying sizes and aspect ratios and are subjected to extreme mechanical and environmental conditions. We describe the settings of hydraulic fracturing (framed by geology), fracturing mechanics and physics, and the critical role that non-Newtonian fluid dynamics and complex fluids play in the hydraulic fracturing process.

INTRODUCTION

Complex fluid: a fluid with a microstructure that is affected by the flow, this perturbed microstructure then gives rise to anisotropic fluid stresses that can modify the flow

Permeability: a geometric constant of a porous material indicating resistance to flow; it incorporates both the porosity and the tortuosity of the porous medium

Pad: particle-free fluid used to initiate the fracture

Hydrocarbons are crucial feedstocks across all sectors of the global economy. The ease of hydrocarbon extraction translates directly into petroleum availability and lower cost for products derived from petrochemicals. Periods of increased worldwide demand, coupled with restricted supply of hydrocarbons, have encouraged and enabled various technological advances to recover oil and gas that is increasingly difficult to remove from the ground. Although a variety of reservoir stimulation techniques are currently used, we describe the process of hydraulic fracturing and the central role that particulate transport by complex fluids plays throughout.

Hydraulic fracturing is not limited to enhancing production of source rocks (also loosely called shales)—as opposed to hydrocarbon reservoirs. It is also used in a majority of oil and gas reservoirs at some point in their lifetime. Fracturing is used in conventional hydrocarbon reservoirs to increase permeability in damaged formations or in formations that exhibit significantly lower production over what could be achieved after fracturing stimulation, e.g., after some decline of production owing to reservoir depletion. It is also used in reservoirs where the intrinsic permeability is too low to yield economical production without it.

Reservoir stimulation by hydraulic fracturing creates additional contact area with the reservoir by pumping a particle-laden fluid into the rock, generating a large pressure relative to the hydrostatic pressure downhole. Because the permeability of the rock is too low to accommodate the flow, and the fluid is (mostly) incompressible, the growing pressure is relieved by the fracturing of reservoir rock generating a new flow path. The first step of fracturing consists of pumping a solid-free fluid, called a pad, that initiates the fracture prior to the introduction of a particle-laden fracturing fluid. This way, risks associated with particles reaching the tip of the fracture (described in the section on Fracturing Fluids) are mitigated. Pumping stops when the desired volume (and fracture extension) is attained or when the pressure required to sustain fracture growth exceeds the available pumping capacity; at this point the well is shut. Over time, the pressure in the fracture and in the formation will equilibrate, following the penetration of the injected fluid into the formation and the closure of the fracture. This process depends largely on the fluid leak-off rate inside the formation and can take several days in low-permeability formations. The fractures do not close completely, as the sand or other proppant carried into the fracture by fluid transport remains and will prop the fractures open. Following this shut-in and leak-off period, the well is reopened and liquid or gaseous hydrocarbons flow out of the reservoir and into the well.

The drilling and hydraulic fracturing process depends critically upon complex fluids. Prior to hydraulic fracturing, a well must be drilled, cased, and cemented. Drilling muds (either aqueous or oil-based) are employed as mechanical stabilizers in the construction of the wellbore to pressurize (via gravitational hydrostatic pressure) the borehole against collapse, cool the drill bit, and carry away rock cuttings. Cements are pumped downhole to form a reinforced casing and (along with metal pipe) isolate sections of the wellbore, providing crucial isolation (1) of the well from the surrounding environment.

The fracturing fluids used in commercial operations are proprietary formulations specific to the geology of the formation and desired treatment, but nearly all contain rigid proppant particles used to hold the newly generated fracture network open after the cessation of flow. Fluids ranging from dilute polymer solutions (i.e., slickwater), polysaccharide solutions (crosslinked and linear), foams (also called energized fluids), micellar fluids (viscoelastic surfactants), and oil-based fluids are loaded with particles of varying sizes, aspect ratios, and densities to achieve the desired combination of chemical and mechanical properties.

Fluid selection for hydraulic fracturing is a design problem. Optimality is economic: Given a hydrocarbon reservoir with a specific set of geological characteristics, what set of fluid properties

will produce the most hydrocarbons for the least cost? This question is straightforward but nontrivial, as it requires a thorough understanding of (*a*) the petrophysical properties of the hydrocarbon reservoir, (*b*) the rheology and formulation costs of the particle-laden complex fluid used in fracturing, (*c*) the fluid–solid interaction driving the hydraulically induced fractures in the anisotropic hydrocarbon reservoir, and (*d*) quantification of risk–reward because no process is 100% reliable. The industry has turned to complex fluids to satisfy this optimization process.

In this review, we focus on the application of complex fluids and non-Newtonian hydrodynamics that governs the hydraulic fracturing of oil and gas reservoirs. This necessarily requires an understanding of hydrocarbon reservoirs, with particular attention to the fluid–solid interactions that occur during the fracturing process, and the nature of reservoir rock (and bounding layers) in general. We first consider a brief history of hydraulic fracturing. This is followed by a discussion of hydrocarbon reservoir petrology and geomechanics. Then, we consider the mechanics of hydraulic fracturing, focusing on the role of fluid, reservoir, and flow properties in determining the fracture geometry. Finally, with the fracturing process quantitatively described, we detail the rheology of complex fluids relevant in the oilfield and explore the wide-ranging and varied types of fracturing fluids that are employed downhole, highlighting the various processes that these complex fluids are involved in during the hydraulic fracturing process.

A Brief History of Hydraulic Fracturing

Hydraulic fracturing is the progeny of reservoir acidizing processes that date back to the late 1800s (2). Acidizing increases permeability and production in reservoirs through the injection of acids directly into the formation, which react with, and subsequently dissolve, carbonates and some sandstones (3, 4). The Van Dyke acidizing patent (2) describes several of the features present in fracturing today: the use of a rubber packer to isolate target areas of the well, the loading of the well with a target fluid (in this case an acid), the pressurization (via an imposed hydrostatic head) of the fluid to improve penetration into the formation, and then the breaking (in this case neutralization) of the fluid with a base. This technique was later expanded upon by Grebe & Stoesser (5), who describe an "organic jellifying material" for use in wells. Grebe & Stoesser (6) further describe a wide range of fluids and fluid-property modifiers in a 1935 article and provide a description of the hydraulic rock-splitting action (**Figure 1**) to increase the effectiveness of acidizing. All of these technologies have descendants in the modern oilfield. Hydraulically driven reservoir deformation was further recognized in water injection and cementing operations throughout the 1940s, as summarized in the monograph by Howard & Fast (7).

The first hydraulic fracturing operation occurred in the Hugoton Gas Field in Kansas in 1947, where a gelled gasoline was used as the fracturing fluid. In the decades since, hydraulic fracturing has grown in scale and importance, following innovations in fluid chemistry and enhancements in pumping capacity. Coupled with the ability to steer a drill bit horizontally over long distances, hydraulic fracturing has enabled the production of source rocks that were not considered producible previously. In the United States alone, it is estimated that 986,000 wells received fracturing treatments between 1947 and 2010 (8); 278,000 of these wells, mostly focused on the development of source rocks, have been drilled since the year 2000. One reason for this uptick is the increased lateral distances that can be drilled; contemporary wells routinely exhibit horizontal laterals (ℓ_b) in excess of 1 mile (9–11). Operators are presently pursuing lengths in excess of 2.25 miles (12). The increase in length is enabled by a decrease in cost per length drilled, which has fallen 57% between 2012 and 2015 (9), current costs (2015) being approximately $1,000/ft, with some variability. Fractures are introduced along these laterals by injecting liquids at high flow rate [in excess

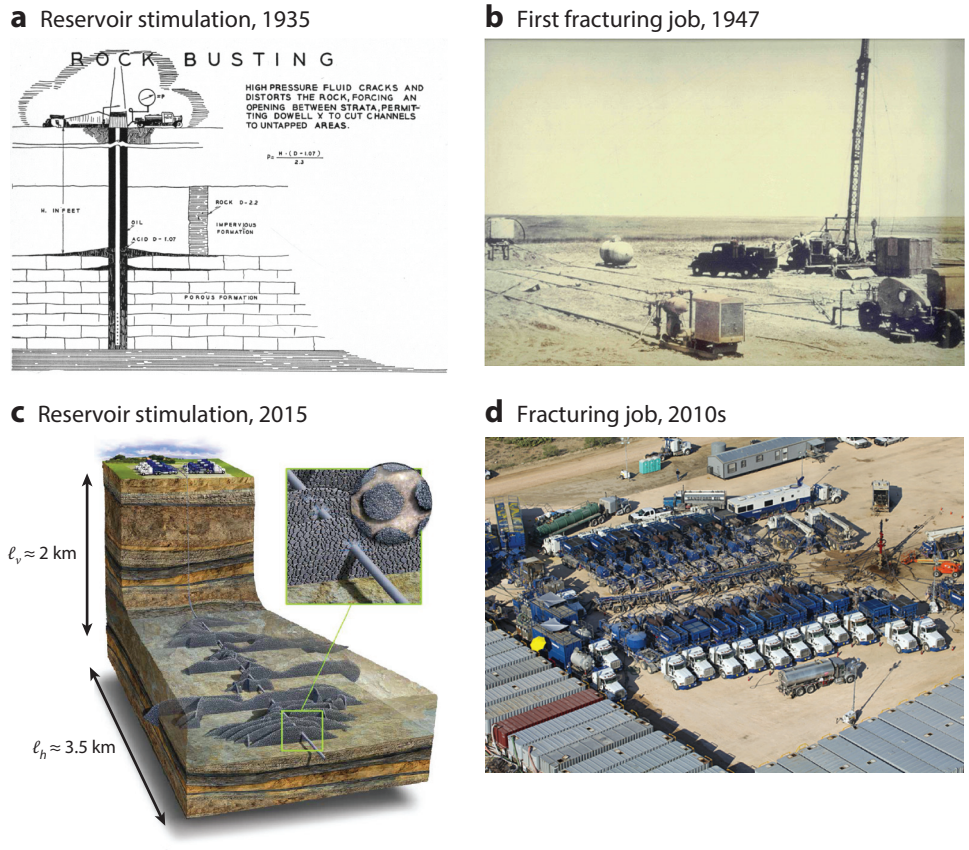

Figure 1

Then and now. (*a*) Schematic diagram of fracturing during an acidizing treatment ca. 1935, from product literature (6). (*b*) The first fracturing operation (1947) in Grant County, Kansas (courtesy Michael B. Smith, credit: Robert C. Fast). (*c*) Schematic diagram of a contemporary fracturing job (courtesy Schlumberger). (*d*) Layout for a contemporary fracturing operation. Pump trucks are arrayed at center, and outlying trailers contain liquids (©CustomAerialImages.com).

of 90 barrels (bbl)/min (13)], stimulating ever-increasing reservoir volumes from isolated wells, recently termed super fracking (14).

Requirements for a Hydraulic Fracturing Fluid

The demands on a hydraulic fracturing fluid are many and are briefly mentioned here, from the sourcing of the material all the way to the cleanup of the fracture after the treatment has stopped. The material for the base fluid should be inexpensive, easy to source, of constant quality, and environmentally harmless. The resulting fluid should be easy to mix/hydrate in water with varying ion content—preferably on the fly—and easy to pump. It should exhibit a low friction pressure drop in a pipe (typical pipe diameter is 4.5″) in the turbulent regime, because it travels along the wellbore for 1–5 miles. When it hits the perforations (aperture of approximately 1″ in diameter connecting the wellbore to the formation) in front of the rock to be stimulated, it should transport proppant through these perforations, which make a 90° angle with the direction of the flow. After

Barrels (bbl)/min: common rate of flow in the oilfield, equivalent to 0.111 $m^3\ s^{-1}$; 1 bbl is equivalent to 42 gallons

going through the perforations, which behave like jets, it should recover viscosity thinned in the high-shear perforation to create fracture width. It should suspend proppant in both dynamic and static conditions and exhibit low leak-off into the formation. After pumping has stopped, it should allow the fracture to close quickly and prevent proppant from settling. After the fracture has closed, it should flow back to the surface easily, without impeding the flow of hydrocarbons either through the matrix where it had previously leaked off or through the proppant pack. Finally, its properties should be tunable to a wide range of downhole temperatures and chemical environments.

Let us note that, for simple Newtonian fluids, many of those requirements are contradictory in nature, e.g., the low friction pressure in the pipe and the high pressure drop in the fracture, or the proppant suspending capability and the ease of proppant pack cleanup. This is the main reason why industry has turned to complex fluids to satisfy these requirements. In spite of this long list of requirements, typical fluids cost less than $1/L (15).

Porosity: a measure of the open space in a material, reported as percent of void space

Kerogen: a nanoporous material, insoluble to both alkaline and organic solvents

HYDROCARBON RESERVOIR PETROLOGY

Sedimentary rocks form the majority of oil reservoirs. Sedimentary rocks can be formed by the successive deposition of fluids and minerals from weathering (mechanical and chemical), evaporation, or biogenic activity, which, over time, become continuous and porous structures, such as sandstones, limestones, and mudstones (16, 17). We shall omit evaporites as they tend to have no porosity or permeability. This sedimentation process occurs as a set of discrete depositions, and the rock is formed by a combination of compaction and cementation (17). Sedimentary reservoirs are porous and present many distinct and identifiable layers, with the precise nature of the sedimentary rock determined by the depositional environment (e.g., a marine shale versus an aeolian dune set), along with the thermodynamic and mechanical history of the reservoir as a whole. The size, shape, and topology of sedimentary structures, along with the thermomechanical properties exhibited locally in the lithosphere, determine many of the pertinent reservoir properties for hydrocarbon production (18). In some sediments, interspersed among clay, sand, and silt are organic materials that will degrade to form oil and gas. Organics trapped within the sedimentary rock experience progressively greater temperatures [increasing at a rate of approximately 2.5°C/100 m (19, 20)] and stresses as the layers travel deeper into the earth (20). The gradual degradation of organics in these source rocks occurs in three stages: diagenesis, catagenesis, and metagenesis, which can be loosely thought of as the heating, cooking, and burning of organic material. Diagenesis occurs in the relatively low-temperature region (<50°C) up to a depth of several hundred meters. Here, organic matter is converted to kerogen (20, 21). Kerogen is acknowledged to exist in three types, delineated by origin, structure (aliphatic versus polyaromatic), and constitution [atomic ratios of hydrogen to carbon and oxygen to carbon (20, 22, 23)]. Oil and gas molecules are derived from kerogen during catagenesis, which occurs at temperatures between 50°C and 150°C. Gas is generated primarily at the higher end of this window. Organic material subjected to yet greater temperatures continues to degrade into dry gas (i.e., methane), with carbon as the ultimate endpoint of thermolysis.

Although kerogen is converted to oil and gas in such formations, called source rocks, traditional drilling operations do not extract hydrocarbons directly from them, as the volume concentration of hydrocarbon is low. Hydrocarbons may undergo primary migration, exiting the source rocks where they originated, and then undergo secondary, buoyancy-driven migration to and within distal porous layers. Eventually, further upward motion of the hydrocarbons is arrested by an impermeable cap (16), and oil and gas are trapped. Conventional extraction targets oil and gas away from source rocks in these secondary porous structures where hydrocarbons are concentrated—hence the term reservoir.

Darcy: permeability carries units of length squared, and is typically cited in Darcies, 1 D = 9.867×10^{-13} m^2; milli- and nanodarcy permeabilities are commonly reported

The most economically favorable reservoirs exhibit large porosities and permeabilities. Porosity, hydrocarbon saturation, and reservoir volume set the available amount of hydrocarbons to be extracted, whereas reservoir permeability sets the relative ease with which the hydrocarbons may be removed. Early oil and gas drilling relied upon the pressure in the earth to expel hydrocarbons directly or with minimal pumping from the wells (primary recovery). If the hydrocarbons are liquid, this production technique produces only a minimal amount of the hydrocarbons in place, and other methods have been developed to recover more of them. For example, because the pressure in the reservoir will decrease as hydrocarbons are produced at the surface, positive displacement of water can then be used to drive hydrocarbons to the surface, known as secondary recovery. Finally, enhanced oil recovery (or tertiary recovery) makes use of chemical additives pumped downhole to coax and recover oil that could not be removed in earlier stages. In all cases, the techniques used are determined by the hydrocarbon content and flow properties of the reservoir—multiple techniques may be used on the same reservoir over the course of its lifetime.

Fluid Flows in Reservoir Rocks

The sedimentary process endows reservoirs with widely varying porosity and permeability (18, 24–26). The initial sedimentation of material forms a porous structure that, through time, is acted upon by chemical and mechanical forces (27–29) to provide (*a*) pores in organic material, (*b*) pores in inorganic material, and (*c*) faults and fractures (30–32); all processes and features yield widely variable porosity and permeability within the reservoir (18, 24–26). Additionally, the sediment settling process results in anisotropic permeabilities such that transport is favored along the sedimentary beds rather than along the direction of deposition (18).

Bernard & Horsfield (33) provide a detailed discussion of inorganic (i.e., mineral-based) and organic (i.e., kerogen-based) pores in mature source rocks, highlighting the change in morphology of the pore network as the source rocks age. Source rocks are distinguished from conventional oil reservoirs by reduced pore size (34) and the role of nanoscale pores within kerogen trapped in the rock. Nanoscale pores in kerogen may not form a formation-spanning connected network but do form a local network on the scale of the organic deposit and are storage sites for gas (29, 35).

Many porous media flows are well-described by Darcy's law,

$$\langle u_i \rangle = -\frac{k_{ij}}{\eta}\frac{\partial p}{\partial x_j}. \qquad 1.$$

Here, u is the local velocity of the pore fluid, and the brackets indicate that this velocity is an averaged quantity. This velocity is proportional to the pressure gradient across the porous media via a permeability tensor, k_{ij}, and a fluid viscosity, η. The quality of reservoirs is often quantified using permeability values, along with the porosity and total amount of organics available for extraction in the reservoir. Bear (36, table 5.5.1) tabulates permeabilities for soils and rocks. Notably, $10 \leq k \leq 10^4$ mD for "oil rocks"; $10^{-1} \leq k \leq 10$ mD for sandstone; and $k \leq 1$ mD is listed as impermeable, or "tight" in contemporary parlance (18). Modern production technology has significantly modified what we consider impermeable; see **Table 1** for more contemporary values and classification.

The linear Darcy relation generally holds for creeping flows of Newtonian fluids. Corrections exist to accommodate larger Reynolds number flows (37), large-scale velocity gradients (38), non-Newtonian effects (39–41), and pressure-dependent permeabilities (24, 37). Despite these corrections, departures from strictly Darcian flow conditions remain an open problem. Complications arise in time-dependent processes, like hydraulic fracturing, where the

Table 1 Reservoir properties for shales, sandstones, and mudstones

Quantity (units)	Range ⟨representative value⟩
Poisson's ratio, ν (–) (18, 61, 62)	0.1–0.5 ⟨0.25⟩
Young's modulus, E (GPa) (18, 61)	5–95 ⟨30⟩
Fracture toughness, K_{IC} (MPa-$\sqrt{\text{m}}$) (61, 63)	0.17–1.73 ⟨1.0⟩
Permeability, k (D)[a] (13, 18)	
Shale gas	$\sim 1 \times 10^{-9}$
Tight gas	$< 0.1 \times 10^{-3}$
Conventional	$< 500 \times 10^{-3}$
Porosity (%) (13)	6–>25[b]
Formation depth, ℓ_v (m) (13)	1,200[M]–4,100[EF]
Formation thickness, h (m) (13)	6[F]–180[B]

[a] $1\text{D} = 9.87 \times 10^{-13}\ \text{m}^2$.

[b] Source rock and tight gas formations are at the low end of this range, conventional formations at upper; depth and thickness range extremes from [B] Barnett Shale, [F] Fayetteville Shale, [EF] Eagle Ford Shale, and [M] Marcellus Shale.

permeability may vary owing to components adsorbed onto the porous matrix from the fluid and/or variations in the pressure difference between the matrix and fluid modulating the pore structure.

The Darcy law (Equation 1) is invalid for gas flows in nanopores, such as those found in kerogen. For these flows, the mean free path (λ) of gas within the pores is large as compared with a characteristic diameter of the pores, d_p, and the continuum Darcy law is strictly inapplicable. The ratio of these lengths forms the Knudsen number, $\text{Kn} = \frac{\lambda}{d_P}$, revealing whether the flow may be described using classical continuum descriptions of transport ($\text{Kn} \ll 1$), whether slip effects must be included ($10^{-3} \leq \text{Kn} \leq 10^{-1}$), or whether free-molecule flow ($\text{Kn} \geq 10^{1}$) must be used to describe gas transport. Several models have been proposed (42–44), starting with the Klinkenberg relation (42), which introduced an empirical permeability, k_s, slip corrected to augment the permeability in the Darcy law, $k_s = k_\infty(1 + K_b/p)$, so that decreases in thermodynamic pressure (p) will augment the permeability; here, k_∞ is a liquid permeability in the same medium, p is the pressure in the pores, and K_b is the Klinkenberg constant.

There is no universal relation to connect the porosity, ϕ, to the permeability, k_{ij}, in rocks or porous media in general. This failure arises from the inherent dependence of the permeability on the detailed geometry of the pores and the distribution of pore sizes, whereas the porosity is a scalar measure that does not include pore-scale information beyond the volume fraction of solids. Strikingly, the permeability in mudstones can vary over three orders of magnitude for the same value of porosity (26)! Despite this limitation, several empirical correlations and analytical models exist (26, 37). The success of the various models depends upon how well the underlying assumptions match physical characteristics of the targeted reservoirs. Katz & Thompson (45), recognizing the self-similarity of pore spaces for several sandstones, developed a predictive permeability model (46), $k = c\ell_c G/G_0$, where c is a numeric constant; ℓ_c is a length scale from mercury injection measurements; and G and G_0 are electrical conductivities of the brine-saturated porous media and brine, respectively. The Katz & Thompson model includes two important components: (*a*) a single characteristic length, ℓ_c, which dominates momentum transport, determined by the inflection point of pressure during a mercury injection test (37), and (*b*) a measure of the pore connectivity through the independent electrical conductivity measurements of brine.

Natural fractures can also contribute to the porosity and permeability. Fractures in rocks form from stresses and natural fluid motion. These fractures and associated fracture networks have been

Volume fraction: typically, $\phi = \frac{V_{\text{solids}}}{V_{\text{total}}}$; industrial specifications of solids concentration are typically in pounds added per fluid volume; pounds added per gallon, ppa, is common

Brine: a salt solution typically at a concentration greater than seawater

identified as major contributors to shale gas reservoirs (47–49); it is therefore desirable in these systems to intersect the natural fracture network during the drilling and hydraulic fracturing process (50). Natural fractures can be characterized by orientation, length, aperture, and roughness (32, 49, 51, 52). Similar to the porous media described above, the natural fracture network can exist in a percolated or unpercolated state and can also be both anisotropic and heterogeneous (51). Percolated fractures within hydrocarbon reservoirs do not necessarily conduct liquids or gases; the fractures may be filled with calcite, or are otherwise sealed (48, 50). Transport models for fractures and fracture networks suffer similar limitations to the porous media discussed previously—the geometry of the networks and individual fractures is strongly variable and typically unknown. These uncertainties aside, individual fractures (53) and fracture networks in porous matrices (52, 54–56) have been analyzed to elucidate estimated flows and permeabilities for Darcy flows.

Despite all the complications associated with the description of multiphase flow in rocks (brine, liquid and gaseous hydrocarbons), one can infer that the total flux that can be drained from a reservoir into a well is a function of the rock permeability, viscosity of the reservoir fluids, pressure gradient, and surface area over which that pressure gradient is applied. Rock permeability is provided by geology and can only be altered locally (e.g., by the injection of reactive fluids). Mobility of the flowing fluid(s) is also given by the nature of the fluids in place and the temperature and pressure conditions in the reservoir—even if it can be modified in some cases by heat (e.g., injection of steam) or injection of surfactants. The magnitude of the pressure gradient that can be applied is also limited, roughly by the difference between the initial fluid pressure of the reservoir and the weight of the hydrostatic column in the wellbore. It is therefore natural to look at the surface area over which a pressure gradient can be applied from the well to the reservoir.

A vertical well drilled in a hydrocarbon reservoir drains the reservoir fluids through a small contact area with the producing layers: The intersection of a 0.2-m-diameter well with a 15-m-thick producing layer results in approximately 10 m^2 of contact area. The magnitude of this contact area can be increased if the well is drilled with a long portion following the producing layer: A 1,000-m lateral drain placed in the same producing layer would have a contact area with the reservoir of approximately 630 m^2. Another means is hydraulic fracturing, the goal of which is to create a large surface area in contact with the reservoir. For example, the creation of a 100-m-long bi-wing fracture in contact with the same reservoir would result in a contact area of 3,000 m^2. If the permeability of the fracture is large enough that the pressure in the fracture is close to that in the wellbore, hydraulic fracturing is extremely effective at promoting flow from low-permeability reservoirs. One of the goals of hydraulic fracturing is thus to create a fracture with a permeability that is infinitely large compared with that of the reservoir that it is draining. Let us remark, finally, that for reservoirs with extremely poor flow characteristics (e.g., with permeabilities of the order of 100 nD or less), lateral drains can be hydraulically fractured to create enough drainage area to concentrate sufficient flow into the wellbore.

Mechanical Attributes of Rocks

Hydraulic fractures arise from fluid–solid interaction resulting in mechanical failure of the formation. The orientation, geometry, and extent of these fractures depend strongly on the intrinsic mechanical properties and state of stress of the reservoir rock. As one wishes to both limit the extension of the created hydraulic fracture to the producing layers of interest and extend the fracture as long as required to obtain the desired producing area, we briefly describe the mechanical system formed by both reservoir rocks and their bounding layers. Reservoir rocks are usually modeled

as linear elastic materials. This is not strictly true for rocks in general (18); elevated temperatures and the presence of pore fluid can lead to plastic rather than elastic failure (57, 58). However, for the hydraulic fracturing process, this has proved extremely effective, mostly because of the loading path followed by the material during the fracturing process.

Within the linear elastic framework, reservoir rocks are characterized by a modulus of elasticity, E, and Poisson's ratio, ν. Note that anisotropy of the rock can also be taken into account. Measurements of these properties can be performed on drill cores removed from the earth, although the cost can be prohibitive, and care must be taken to preserve the in situ rock conditions (water/fluid content, overburden pressure) when tests are performed (58). Sonic logging tools permit direct interrogation of rocks downhole (59), accomplished by measuring the propagation speed of waves through rock and using the density to recover elastic moduli and Poisson's ratio. These and other dynamic methods typically yield larger values of both the Poisson's ratio (60) and elastic moduli (60, 61) as compared with measurements using static methods, as would be done in the lab on core samples in gradual compression. Correlations have been developed to allow the transformation of the parameters obtained under small-strain/large-frequency (dynamic) conditions to parameters corresponding to large-strain/low-frequency (static) conditions required for modeling the hydraulic fracturing process. Beyond variations in these values owing to test type and configuration, mechanical properties also vary substantially from reservoir to reservoir and within rock layers forming the reservoirs, as presented in **Table 1**, and in the references cited therein. Tensile failure in rocks can be characterized by a fracture toughness, K_{IC}. Contrary to the variation in the elastic parameters, the value of the fracture toughness does not vary strongly between rocks and is of the order of 1 MPa$\sqrt{\text{m}}$.

The lithostatic stress determines the orientation and, along with rock properties and the injection pressure, the extent to which the reservoir may be fractured. Lithostatic stresses can be highly anisotropic. These stresses arise chiefly from the weight of rock atop any given point in the reservoir. Typically, the lithostatic stress is highest in the vertical direction (aligned with gravity), with a horizontal stress that varies as a function of depth. Brown & Hoek (64) tabulate the ratio as $r = \frac{\sigma_v}{\sigma_h}$ and write the empirical bounds as $\frac{100}{z} + 0.3 \leq r \leq \frac{1500}{z} + 0.5$, where z is the vertical depth in meters. Because the density of rocks is not a strongly varying quantity, the vertical stress at the same vertical depth z correlates with $\sigma_v = 27 \times 10^3 z$, with σ_v in pascals. Complexities arise owing to the combination of gravitational body forces as well as tectonic activity and thermal and fluid pressure effects on the potentially complex geological structure hosting the reservoir of interest. For example, these forcing mechanisms can vary the relative dominance of the horizontal and vertical stresses, to the point where the (once) dominant vertical stress becomes subordinate.

Let us note that the (possibly large) variations of both mechanical (including the lithostatic stress state) and flow properties from one layer to the next, along with often poorly constrained variations of these properties along a layer, 100 m away or more from the wellbore, put a very strong requirement of robustness on the design of a hydraulic fracture to such variations, and thus on the fluid systems that will be used to create them.

MECHANICS OF HYDRAULIC FRACTURING

The mechanics of fracture generation and arrest have been studied extensively in the decades following the first field tests. Because the choices of fluid and pumping rate are the main design levers to achieve the desired fracture geometry in a given geological setting, these studies have highlighted the (often conflicting) requirements placed on hydraulic fracturing fluids. In the following section, we review the phenomena specific to the fluid–solid interactions in hydraulic fracturing.

Fracture Orientation and Geometry

Mineback: excavation of a fractured formation to measure fracture geometry and extent

The fracture orientation conspires with the flow properties of the reservoir rock to determine the efficacy of the fracturing operation. Reservoirs have anisotropic permeability. The permeability is generally smallest through the plane of bedding; thus, the desired flow path is perpendicular to the formation bedding. The orientation of hydraulic fractures is predominantly controlled by the in situ stresses of the reservoir (61, 65), and fractures tend to propagate perpendicular to and open in the direction of the minimum compressive stress. Hubbert & Willis (66) clearly demonstrated this in a set of laboratory experiments using a gelatin mold as the reservoir and liquid plaster as the fracturing fluid; after curing of the plaster, fractures of vertical and horizontal orientation were observed, consistent with compressive stresses applied to the mold. A study of the rank ordering of the stresses in the reservoir is thus a prerequisite to decide whether hydraulic fracturing can be applied. If the minimum stress is near perpendicular to the reservoir bedding, a hydraulic fracture parallel to bedding will be created regardless of the fluids being used. Thus, during production, flow through the fracture face proceeds along the direction of minimal permeability, limiting the benefit of the fracturing process.

Preexisting fractures, joints, and faults can, however, redirect or modify the propagation direction of induced fractures (65, 67–70). In conventional reservoirs, this reorienting effect is not generally strong enough to override the global fracture orientation that is dictated by lithostatic stresses (71). In unconventional reservoirs (often fractured source rocks), the interaction between the hydraulic fracture, the bedding planes, and the preexisting fractures and faults has tremendous importance, directly impacting the amount of stimulated reservoir area. Whether a hydraulic fracture ignores a preexisting fracture/bedding plane is a function not only of the geomechanical setting but also of the fracturing fluid (72), which adds another dimension to the selection of fracturing fluids.

Measurement of hydraulic fracture geometry is challenging, requiring remote downhole or direct measurement from mineback experiments (71). A wide range of fracture lengths, widths, and heights are reported in the petroleum literature and, along with treatment and reservoir parameters (50), are highly variable (73, 74); see **Tables 1** and **2** for ranges of natural and engineered parameters.

The width of the fracture is the smallest lengthscale in the system; it is largest at the wellbore, where the pressure is greatest, and decreases toward the fracture tip. Cipolla et al. (74), in a discussion on the relation between fracture complexity and dimension, provide fracture widths varying from 2.5 mm to 185 mm when fluids ranging from waterfrac/slickwater [basically dilute polymer solutions with $\eta \sim$ O(1) mPa-s] to gel-like fluids [$\eta \sim$ O(100–1,000) mPa-s] are used. The fracture length is typically hundreds to more than a thousand meters, and the fracture height may be 50–100 m. The flow may branch during stimulation, forming a tortuous network of fractures. Treatments of the same reservoir with different viscosity fluids have been observed to follow the general expectation that lower-viscosity fluids produce longer (and thinner) fractures than thicker gel-based systems (74). The footprint in a reservoir of multiple fracture treatments staged along a horizontal wellbore can be inferred from microseismic measurements (75), where the seismic activity is assumed to coincide with fracture progress.

Simple Models for Hydraulic Fracture Geometry

One of the strong peculiarities of hydraulic fracturing is the robust coupling between fluid flow, reservoir deformation, and fracture growth. We discuss here insights provided by the two-dimensional Perkins-Kern-Nordgren (PKN) and radial and Khristianovic-Geertsma-de Klerk

Table 2 Operational scales in hydraulic fracturing

Quantity (units)	Range	Remarks
Fracture height (m), h	10–100	Set by the rock formation and local stresses
Fracture width (mm), w	2–185	2–10 is typical
Fracture length (m), ℓ	100–1,000	Can form complex network
Fluid viscosity (mPa-s), η	1–1,000	Impacts fracture width, length, network complexity
Proppant diameter (μm), a	100–850	Highly variable and polydisperse
Proppant concentration (%), ϕ	0–20	Variable during injection, correlated with η
Fluid injection rate ($m^3\ s^{-1}$), Q	0.05–0.27	20–100 bbl/min
Shear rate (s^{-1}), $\dot{\gamma}$	0–1,000	The magnitude of $\dot{\gamma}$ is important for controlling proppant settling and the local fluid rheology
$\mathrm{Re_w} = \rho_f w^2 \dot{\gamma}/\eta$	0–5,000	Flow can be turbulent in wellbore, where $\mathrm{Re}_r \sim 10{,}000$
$Wi = \lambda\dot{\gamma}$	0–1,000	Difficult to quantify at downhole temperature, where the relaxation time λ may be hard to determine
$\mathrm{Re_p} = \mathrm{Re_w}\frac{a}{w}$	$\leq$100	From upper limit on $\mathrm{Re_w}$
$Pe_a = 6\pi\eta\dot{\gamma}a^3/(k_B T)$	$>10^3$	Proppant is noncolloidal and viscous stresses dominate

(KGD) models. These models are physical and geometrical simplifications of the full transient and three-dimensional fluid–structure interaction problem. These approaches, following a variety of assumptions, provide analytical solutions to the fracture problem illustrating the dominance of dissipation mechanisms and how these mechanisms translate to fracture geometry and fluid design. Regardless of their simplifying assumptions, these models are used to validate hydraulic fracture simulations (76) and inform fracturing job design where applicable.

PK, PKN, KGD, and radial fracture models. Models by Perkins & Kern (PK) (77), later modified by Nordgren (78) (PKN), and a plane-strain model by Khristianovic (79) and Geertsma & de Klerk (80) (KGD), along with a radial model (80, 81), all present simplifying assumptions in the state of strain and dissipation. Many of these assumptions are revisited in later refinements.

In the PKN model, a bi-wing fracture with an elliptic cross-section emanates from the wellbore. The height h (ellipse major axis) of the fracture is set a priori to a constant. The fracture width, w (ellipse minor axis), is determined via a plane-strain elasticity relation (82):

$$w(x,t) = 2h\frac{(1-\nu^2)}{E}(p(x,t) - \sigma_\perp). \qquad 2.$$

Here, the pressure in the invading fluid, $p(x, t)$, balances against the far-field solid stress, $\sigma_\perp$, in the formation and compression of the linear elastic reservoir with Poisson's ratio, ν, and Young's modulus, E. Note that only the difference is significant, $\Delta p = p(x,t) - \sigma_\perp$. The plane-strain condition in each vertical plane constitutes a crucial simplifying assumption—the elliptical deformation profiles in the direction of the fracture propagation become uncoupled. Whence, the fracture width (minor ellipse axis) is determined uniquely by the local fluid pressure, reservoir stress, Young's modulus, and Poisson's ratio at each location along the fracture. Furthermore, in this model, fracture behavior at the propagating tip is completely neglected; the fracture toughness does not appear in the solution.

The pressure in the fluid is given by a lubrication approximation to the Navier-Stokes equations, inherently assuming laminar flow prevails. Here, the pressure drop along the fracture depends linearly on the viscosity, η, and flow rate, while depending more strongly on the fracture width,

so that,

$$\frac{\partial \Delta p}{\partial x} = -\frac{64\eta}{\pi}\frac{Q}{w^3 h}. \quad 3.$$

Note that the flow rate in the fracture, Q, and the width, w, are functions of position and time. The flow rate varies in time and space along the fracture by any combination of (*a*) a change in pumping rate (or flow schedule) at the surface, (*b*) leak-off of fluid through the porous fracture walls into the formation, and (*c*) accumulation in the fracture as the width varies in space and time.

With the assumption of an incompressible fluid, a statement of mass conservation connects the fracture width (Equation 2), pressure drop (Equation 3), flow schedule, and other system properties to enable prediction of fracture geometry as a function of time:

$$\frac{\partial Q}{\partial x} + q_L + \frac{\pi}{4} h \frac{\partial w}{\partial t} = 0. \quad 4.$$

The first term accounts for the change in volumetric flow as a function of position along the fracture; the second term, q_L, is the volumetric flow rate of leak-off per unit fracture length from the fracture into the formation; and the final term accounts for the expansion or contraction of the fracture width as a function of time.

The early work by Perkins & Kern (77) assumed $\frac{\partial Q}{\partial x} = 0$, neglecting both changes in fracture aperture and leak-off. Nordgren (78) recognized that both leak-off and evolution of the fracture aperture must be included, resulting in a nonlinear partial differential equation for the fracture width:

$$-\frac{1}{128\eta}\frac{E}{1-\nu^2}\frac{1}{h}\frac{\partial^2}{\partial x^2}(w^4) + \frac{4}{\pi}\frac{1}{h}q_L + \frac{\partial w}{\partial x} = 0. \quad 5.$$

This equation is subject to the initial condition $w(x, 0) = 0$ and the distal boundary condition $w(x, t) = 0$ when the coordinate $x \geq \ell(t)$, where $\ell(t)$ is the fracture length at arbitrary time. The problem is closed by an additional boundary condition on the flow into the fracture as a function of time. In the absence of leak-off, the fracture length and width and pressure difference in the fracture have all been determined analytically for a constant injection rate at the wellbore (83). These results are shown in **Table 3**. Note that this model corresponds to the limiting case of a height-constrained fracture—perfectly contained—with a length much larger than the height, akin to a tunnel crack.

Models for other limiting cases include that of Geertsma & de Klerk (80), incorporating work from Khristianovich (79), who developed models that include the influence of the fracture tip to

Table 3 Perkins-Kern (PK), Perkins-Kern-Nordgren (PKN), Khristianovic-Geertsma-de Klerk (KGD), and radial model predictions for an impermeable formation ($q_L = 0$), following References 80, 83, and 221

Model	$\ell(t)$, $R(t)$	w(0,t)	Δp
PK[a], PKN[b]	$C_1\left(\frac{EQ^3}{2(1-\nu^2)\eta h^4}\right)^{1/5} t^{4/5}$	$C_2\left(\frac{2(1-\nu^2)\eta Q^2}{Eh}\right)^{1/5} t^{1/5}$	$C_3\frac{1}{h}\left(\frac{E^3 Q\eta \ell(t)}{8(1-\nu^2)^3}\right)^{1/4}$
KGD[c]	$C_1\left(\frac{EQ^3}{2(1-\nu^2)\eta h^3}\right)^{1/6} t^{2/3}$	$C_2\left(\frac{2(1-\nu^2)Q^3\eta}{Eh^3}\right)^{1/6} t^{1/3}$	$C_3\frac{1}{2h}\left(\frac{E^3 Q\eta h^3}{8(1-\nu^2)^3\ell(t)^2}\right)^{1/4}$
Radial	$0.64\left(\frac{EQ^3}{2(1-\nu^2)\eta}\right)^{1/9} t^{4/9}$	$1.36\left(\frac{\eta^2 Q^3(\nu^2-1)^2}{E^2}\right)^{1/9} t^{1/9}$	$3.38\left(\frac{E^6\eta^3}{(\nu^2-1)^6}\right)^{1/9} t^{-1/3}$

Coefficients for single and bi-wing fractures (single wing, bi-wing).
[a] $C_1 = (0.60, 0.395)$, $C_2 = (2.64, 2.00)$, $C_3 = (3.00, 2.52)$.
[b] $C_1 = (0.68, 0.45)$, $C_2 = (2.50, 1.89)$, $C_3 = (2.75, 2.31)$.
[c] $C_1 = (0.68, 0.48)$, $C_2 = (1.87, 1.32)$, $C_3 = (2.27, 1.19)$.

describe the fracture geometry. As before, laminar flow is assumed within a fracture embedded in an isotropic linear elastic solid. Models were developed for both linear (KGD) and radial fractures. The KGD case considers plane strain along the propagation direction and corresponds to the limiting case where the height of the fracture is much larger than its length, whereas the radial case corresponds to the propagation of a hydraulic fracture in an infinite isotropic medium. In each, the fracture width is determined nonlocally by the fluid pressure and far-field stress. Both are constrained by a smooth fracture closure condition (79, 84), for the radial case: $\frac{\partial w}{\partial r}\big|_{r=R(t)} = 0$, although other asymptotes that incorporate the mode 1 stress intensity factor can be considered, for example, $w \sim \sqrt{\frac{32}{\pi}}\frac{K_1(1-\nu^2)}{E}\sqrt{R-r}$ for the radial case (85). We present results for both the linear and radial fractures (**Table 3**) but consider only the radial fracture in detail, as it is the simplest, but most complete, model for practical applications.

The radial model assumes a penny- (or disc-)shaped fracture of radius R, emanating from a well of radius r_w, with a local width, $w(r)$. The closure condition places a constraint on the pressure,

$$\int_{r_w/R}^{1} \frac{sp(s)}{\sqrt{1-s^2}} ds = \sigma_\perp. \qquad 6.$$

This mechanical condition is combined with a description of the hydrodynamics in the fracture. A piecewise pressure profile is assumed in the fracture to satisfy Equation 6. It consists of two regions: a section with logarithmic pressure decay owing to viscous dissipation and expanding flow area along the radius and a zero-pressure region near the fracture tip:

$$\begin{aligned} p(r) &= p(r_w) - \frac{6\eta Q}{\pi \bar{w}^3} \ln \frac{r}{r_w}, \quad r_w \le r < r_c. \\ p(r) &= 0, \quad r_c \le r \le R. \end{aligned} \qquad 7.$$

Here, $\bar{w}$ is the average fracture width. Equation 7 implies a gradual decrease in pressure outward along the fracture followed by a severely dissipative region near the tip, and a zero-pressure region to satisfy the tip closure condition. The length scale corresponding to this dissipation region, r_c, is found through the tip closure condition (83), $r_c/R \approx 1 - 0.368[\frac{E^3\eta Q}{\sigma_\perp^4(1-\nu^2)^3R^3}]^{1/3}$.

The pressure, fracture width, and radius are determined via an analysis of the strain induced by the pressure and the hydrodynamic model of laminar flow in a radial fracture (80, 83). These results are shown in **Table 3**, where both storage and leak-off are neglected. The pressure varies weakly with radius, except near the tip through the step function in Equation 7.

Leak-off in the PKN and radial models. Substantial complications in the mass conservation statement for both the PKN and radial models are introduced by fluid leak-off into the formation. The leak-off term q_L is often given by the Carter law [originating in an appendix to a conference proceeding by Howard & Fast (86)], and is typically of the form $q_L = \frac{2bC_L}{\sqrt{t-t_{\exp}}}$ when the height is constant. The leak-off rate varies as a function of the elapsed exposure time at the fracture face, $t - t_{\exp}$, where $t_{\exp}$ is the time when fluid exposure occurs on the newly fractured rock; this decrease in leak-off is due to the progressive buildup of a hydraulic resistance in the reservoir to the invasion of the fracturing fluid, be it by simple diffusion gradient or by the formation of a filter cake, either at the fracture wall or in the near-fracture region of the reservoir. In the case of filter cake formation, material is deposited on the wall and/or within the pores. The leak-off coefficient, C_L, typically depends on the fluid viscosity, the pressure difference between the fluid in the fracture and the far-field pressure of the fluid in the pores, and the permeabilities of the filter cake and reservoir. Models using Darcy's law can be used to construct the leak-off coefficient (37). However, because the process relies on the detailed pore-scale structure of the rock averaged

over large surfaces where the variation of such details is unknown, the leak-off rate is typically determined experimentally, both in the field and in the laboratory.

The fracture problem with leak-off can be solved numerically in the general case, as Nordgren (78) originally did for the PK model. These results indicate a matching at long and short times with restricted versions of the full mass-transport equations. Nordgren's characteristic time scale, $t^* = \pi^2(\frac{(1-\nu^2)\eta Q^2}{64C_L^5 bE})^{2/3}$, developed by making the PKN equation set dimensionless, indicates early times, $t < t^*$, where leak-off is minimal and late times, $t \gg t^*$, where fluid loss to the formation is significant. Limiting results for the fracture length, width, and pressure following this early/late time approach appear in work by Nordgren (78) and Geertsma (83) for the PKN fracture.

The rapidly increasing complexity of solving the coupled equations for this nonlinear moving boundary problem leads very quickly to fully numerical solutions, be it for the radial geometry (87) or for more complex planar or even fully three-dimensional geometries (88). Another approach to the problem is to focus on what is happening at the tip of the fracture. Here, the coupling of the various processes at play yields a series of multiscale solutions highlighting mechanisms that control energy dissipation as the fracture propagates.

Asymptotic Solutions

Following the KGD and radial results outlined above, Spence & Sharp (89) more carefully approached the fracturing fluid–structure interaction problem through a similarity solution for flow into a penny- (or lens-)shaped cavity. Related approaches have been adopted by Spence & Turcotte (90) to explore the formation of dykes (magma-driven fractures), and also for studying buoyancy-driven propagation [Spence, Sharp & Turcotte (91) and Lister (92)]. These analyses highlight the importance of various physical processes in determining the final geometry of the fracture and, crucially, the localization of processes at the fracture tip.

Lister (92) notes that when the crack tip is saturated with liquid, large pressures are required to fill the fracture; instead, it can be supposed that there is a region of fluid lag with inviscid material filling the remainder of the fracture between the liquid front and fracture tip. Desroches et al. (93) further discussed this distinction between fluid filling and fluid lagging the fracture tip, indicating that fluid approaching the fracture tip implies a solution of zero stress intensity factor ($K_1 = 0$) in the leading order term, with a stress singularity weaker than predicted by linear elastic fracture mechanics. The dominant dissipation mechanism is due to the pumping of viscous liquid into the fracture tip (Poiseuille flow) rather than the fracture process itself.

The strength of the singularity at the crack tip indicates the dominant physical process (94–97). In 2004, Detournay (95) summarized this work for fracturing in impermeable rock, $q_L = 0$, considering both the radial and plane-strain KGD fractures. Absent of leak-off, a dimensionless toughness $\mathcal{K} = (\frac{L_m}{L_k})^p$ identifies whether the fracture process is dominated by viscosity ($\mathcal{K} \leq 1$) or fracture toughness ($\mathcal{K} \geq 4$). The exponent p is 5/2 and 3/2 for the radial and KGD fracture, respectively. Expressions for L_m and L_k, along with the controlling ratio $\mathcal{K}$, are presented in **Table 4**. These scalings show that the KGD fracture is dominated by the same physics for all time, as determined by the temporal invariance of the parameter $\mathcal{K}$. The radial fracture exhibits a $t^{\frac{1}{9}}$ time dependence, indicating that the dominant dissipation mechanism changes from viscous dissipation to fracture toughness dominated at long times.

Asymptotics with leak-off. Inclusion of leak-off for permeable formations adds an additional dissipation mechanism; relaxation of the impermeability condition permits fluid accumulation

Table 4 Length scales for viscosity and toughness in Khristianovic-Geertsma-de Klerk (KGD) and radial models under constant injection rate Q, from Reference 95

	L_m	L_k	$\mathcal{K}$
KGD	$\left(\frac{E'Q}{\eta'}\right)^{1/6} t^{2/3}$	$\left(\frac{E'Q}{K'}\right)^{2/3} t^{2/3}$	$\frac{K'}{(E'^3\eta' Q)^{1/4}}$
Radial	$\left(\frac{E'Q^3}{\eta'}\right)^{1/9} t^{4/9}$	$\left(\frac{E'Q}{K'}\right)^{2/5} t^{2/5}$	$\frac{K'}{(\eta'^5 Q^3 E'^{13})^{1/18}} t^{1/9}$

Here, $\eta' = 12\eta$, $E' = E/(1-\nu^2)$, and $K' = 4(2/\pi)^{\frac{1}{2}} K_{IC}$. K_{IC} is the fracture toughness.

in the formation, in addition to the fracture. Lenoach (98) considered leak-off with a viscosity-dominated fracture, and Bunger et al. (99) considered leak-off in the toughness-dominated case. Subsequently, Garagash et al. (97) presented a generalized approach where leak-off and storage in the fracture, along with viscous and toughness losses, are all active within the fracture and at the tip. This unifying approach verifies that previous analyses (as detailed in Reference 97) are obtained as limiting cases of the general problem. Tip asymptotics can be used to indicate the dominant mechanisms in planar fracture propagation. Detournay (100) provides a recent review highlighting the multiscale and time dependence of the leading phenomena at play during creation of a hydraulic fracture. Verifying the regime in which a hydraulic fracture will be propagating is of crucial importance in the design of laboratory tests and small-scale experiments to understand the behavior of a hydraulic fracture. Improper scaling of the dominant physics yields results that are purely of academic interest and cannot be practically exploited.

Transport of Solids in Hydraulic Fracturing

Solid particles are injected to sustain fractures of the desired geometry against closure stresses imposed by the reservoir. A straightforward dimensional analysis provides insight to the transport phenomena at play during creation and propagation of the hydraulic fracture. The geometry of the fracture (w, h, ℓ), the injection rate (Q, or shear rate $\dot{\gamma}$), fluid rheology (chiefly viscosity η, relaxation time λ, and fluid density ρ_f), and proppant properties (solids volume fraction ϕ, radius a, density ρ_s) frame the geometric and dynamic scales. Application of the Buckingham Pi theorem to the variables $(w, h, a, \phi, \rho_s, \rho_f, \eta, \lambda, \dot{\gamma})$ forms a set of six dimensionless groups, two purely geometric ($\Pi_1 = w/h$, $\Pi_2 = w/a$), three dynamic ($Re_w = \rho_f w^2 \dot{\gamma}/\eta$, $Wi = \lambda\dot{\gamma}$, $Sk = \Delta\rho a w\dot{\gamma}/\eta$), and the volume fraction, ϕ. Here, $\Delta\rho = |\rho_s - \rho_f|$ is the density difference. The geometric parameters define the aspect ratio of the fracture (w/h) and the aperture as measured by the particle size (w/a). The relevant dynamic conditions of the flow are indicated by the dominance of viscosity versus inertia through the Reynolds number (Re), the flow timescale versus the fluid relaxation time through the Weissenberg number (Wi), and the importance of particle inertia in unsteady flows via the Stokes number (Sk). The shear rate, $\dot{\gamma}$, varies throughout the fracture and can be computed from the flow rate and the fracture geometry. Here, we choose the simple relation, $\dot{\gamma} = Qw^{-2}h^{-1}$, assuming flow in a slit. Note also that a particle-based Reynolds number can also be defined, $Re_{\mathrm{p}} = \Pi_2^{-1} Re_{\mathrm{w}}$.

Additional physical variables give rise to additional dimensionless groups. These groups will reflect the important physics of the transport process and the rheology of the complex fluid in the fracture. A Shields parameter (see section on Particle Settling), for example, captures the ability of a slickwater treatment to transport proppant particles settled along the bottom of a fracture. Further, we could quite reasonably specify a particle settling velocity to compare against the flow

velocity, a wall roughness or channel bend radius to compare against the channel width or particle size (53, 101), a thermodynamic energy scale to compare against viscous dissipation around the particle (102), or additional timescales for the fluid rheology or pumping schedule.

Implications for Fracturing Fluids

These models highlight expected geometric and dynamical scalings associated with fluid selection. Parameterization of the particle-laden fracturing fluid is often relegated to the magnitude of the viscosity only, occasionally also capturing shear-rate dependence (93). The fracture geometry depends weakly on the viscosity: For a PKN fracture geometry, the length scales with the viscosity as $\ell \sim \eta^{-1/5}$, width as $w \sim \eta^{1/5}$, and pressure as $\Delta p \sim \eta^{1/4}$. Fluid viscosity must thus be varied by orders of magnitude to significantly alter length and width. However, assuming simple Darcy flow into the formation, the leak-off will scale as $C_L \sim \frac{1}{\sqrt{\eta}}$, and Nordgren's crossover timescales as $t^* \sim (\eta C_L^{-5})^{2/3} \sim \eta^{7/3}$, indicating a strong viscosity dependence for leak-off. Settling also depends strongly on the viscosity; the Stokes settling velocity of a suspension with volume fraction ϕ scales as $u \sim \eta^{-1}(1-\phi)^5$ (103).

These scaling considerations highlight contradictory fluid requirements and the need for complex fluids in hydraulic fracturing. The demands on the fluid are significant: A fracture job designed to generate a large fracture width (placing large amounts of proppant per fracture area) will require a high-viscosity fluid during injection. As a result, the fluid will exhibit low leak-off and result in a long fracture closure time. This long closure time favors proppant settling, leaving the top part of the fracture mostly unpropped and prone to closure. This can decrease the final contact area between the fracture and the reservoir. Thus, a large viscosity is required during pumping and a small viscosity is required to favor leak-off after shut-in. Further examples of competing requirements include (*a*) low pressure drop in the pipe and the simultaneous creation of fracture width; (*b*) low leak-off during fracture creation but fast fracture closure after pumping has stopped, with low damage of the rock permeability (104); and (*c*) transport of solid particles while providing maximum permeability of the placed proppant pack to hydrocarbon fluids.

Three main routes exist to optimize between these conflicting requirements. A train of fluids is often used; for example, creation of fracture complexity requires a thin, solids-free fluid. A slurry created by adding solids to the base fluid will not create enough fracture width to admit large concentrations of proppant particles. Therefore, a sequence of at least two different fluids is preferred: a low-viscosity fluid to propagate the leading edge of the fracture, followed by a particle-laden fluid with a larger viscosity. A second route to address this fluids design challenge is the use of additives to decouple fluid properties; for example, starch particles can be added to control leak-off. A third route is to use fluids whose properties can be altered with time and temperature.

FRACTURING FLUIDS

The formulation and properties of hydraulic fracturing fluids vary greatly in response to performance requirements that are set by constraints on the surface and downhole (105, 106). The choice of fracturing fluid is largely set by reservoir properties, which are strongly variable across different reservoirs (if not within a particular reservoir). Thus, a complex design of the base fluid must be performed for each job. Today, this design is largely empirical and is guided by return on experience, even as numerical simulators are used to inform the design of hydraulic fractures.

As described in the above section Requirements for a Hydraulic Fracturing Fluid, fracturing fluid design is highly constrained, and successful fluid designs are complex. Additives, both chemical (such as polymers) and physical (e.g., spherical particles and fibers), endow the fluid with a non-Newtonian response in which the stress varies nonlinearly with the shear rate, and changes also as a function of mechanical (and thermodynamic) variables. Other important non-Newtonian characteristics include strain-dependent stresses, viscoelasticity, thixotropy, and a finite yield stress during shearing, among others (107, 108). Importantly, non-Newtonian fluids can also exhibit normal stress differences that are not observed in Newtonian fluids; normal stresses give rise to several important phenomena, including elastic tension along streamlines (107, 109), particle migration (110, 111), and elastic instabilities (112, 113). The various processes described here, and how they manifest in the fracturing process, are shown schematically in **Figure 2**.

The majority of fracturing fluids used today are aqueous (8). Diesel, alcohol, and other organic-based fluids, although desirable because they tend not to cause formation damage and are easily viscosified, tend not to be used because they are hazardous to pump at high pressures and in large volumes (106). Both aqueous and organic fluids can be foamed (or energized), and most are eventually filled with proppant. Owing to the proprietary nature of fracturing fluids, definitive information on components and concentrations is not generally available. Also, the chemical structure of components can be ambiguous. Reviews by Barati & Liang (114), Montgomery (15, 106), Gulbis & Hodge (115), and Ely (105) describe many chemical and physical properties of commonly used fracturing fluids.

Polysaccharide-Based Fluids

Polysaccharide-based fluids are inexpensive and effective viscosifiers, achieving desired fracture widths and reduced proppant settling. Most of these materials are well studied (116). Guar is the most common polysaccharide used in hydraulic fracturing (15). It is mostly soluble in water (the residue varies depending on the source and preparation) and biodegradable, presents low health concern (it is commonly used as a food additive), and can be readily broken. Xanthan gum and cellulosic materials are also used. Xanthan is less common owing to its higher cost. Materials modified from cellulose (which is itself not soluble in water) are also used because they have fewer impurities than guar (115) and easily form gels when derivatized (e.g., hydroxyethyl cellulose) (116). Here, we focus on guar exclusively, as guar-based fluids can answer all of the requirements enumerated above and have been the fracturing fluid of choice for decades.

Uncrosslinked, or linear, guar consists of a mannose backbone substituted with galactose side chains to an average ratio of 1.8:1 mannose:galactose (117). Uncrosslinked guar behaves as a viscoelastic shear-thinning fluid (118). The galactose units are commonly modified (115) to change (*a*) the solvation properties of the guar, (*b*) the availability of crosslinking sites and chemistries, and (*c*) the performance of the material at elevated temperature. Borate and various metal ions crosslink the linear material to form a physical or chemical gel. Crosslinking with borate requires elevated pH ($\gtrsim$7.5) (114, 119), resulting in a dynamic ionic bond in which the borate ion connects *cis*-diols on the galactose. The dynamics of these crosslinks have been studied extensively (120, 121), and they give rise to a classical Maxwell-like linear viscoelastic response of the material (119) and a more viscous solution (as compared with the uncrosslinked case) in steady shear that can also display shear thickening above a critical shear rate (122). Crosslinking with metal ions is performed over a larger range of pH (depending on the ion) (115), and gels crosslinked with zirconate can tolerate a higher downhole temperature than those crosslinked with borate (114). Because the metal crosslinked guar forms a chemical gel, shearing disrupts the bonding network, and the gels do not completely reheal (114, 123). Temperature and pH accelerate the crosslink

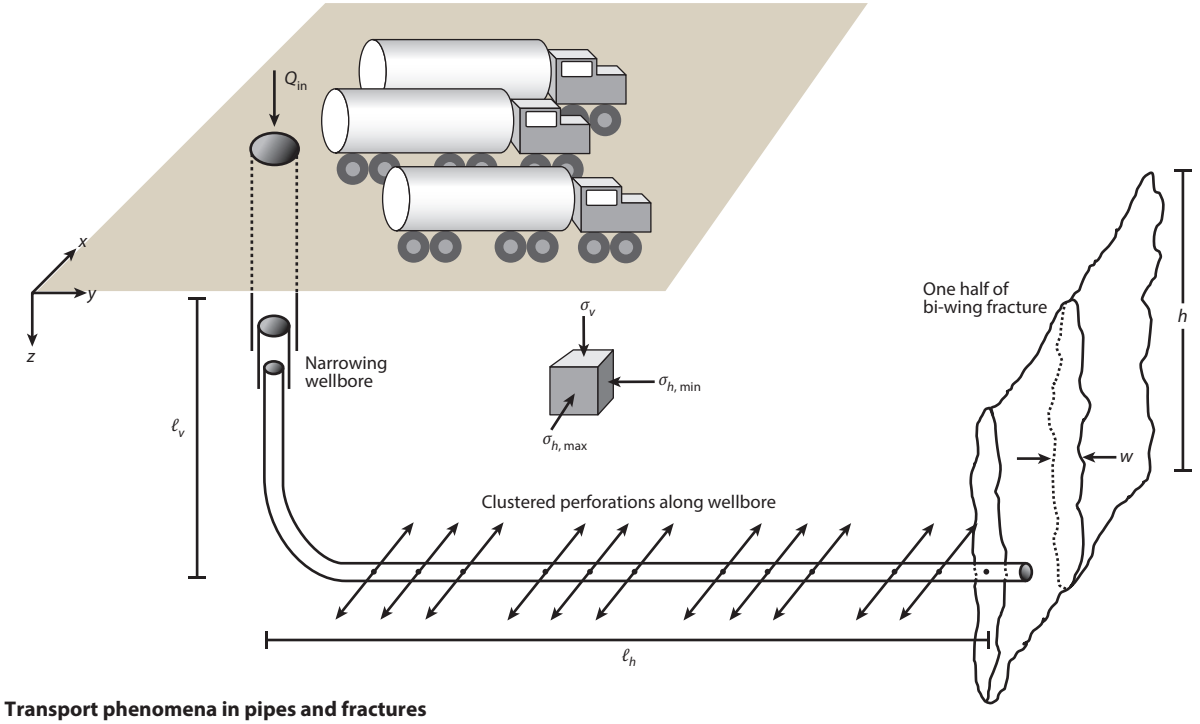

Transport phenomena in pipes and fractures

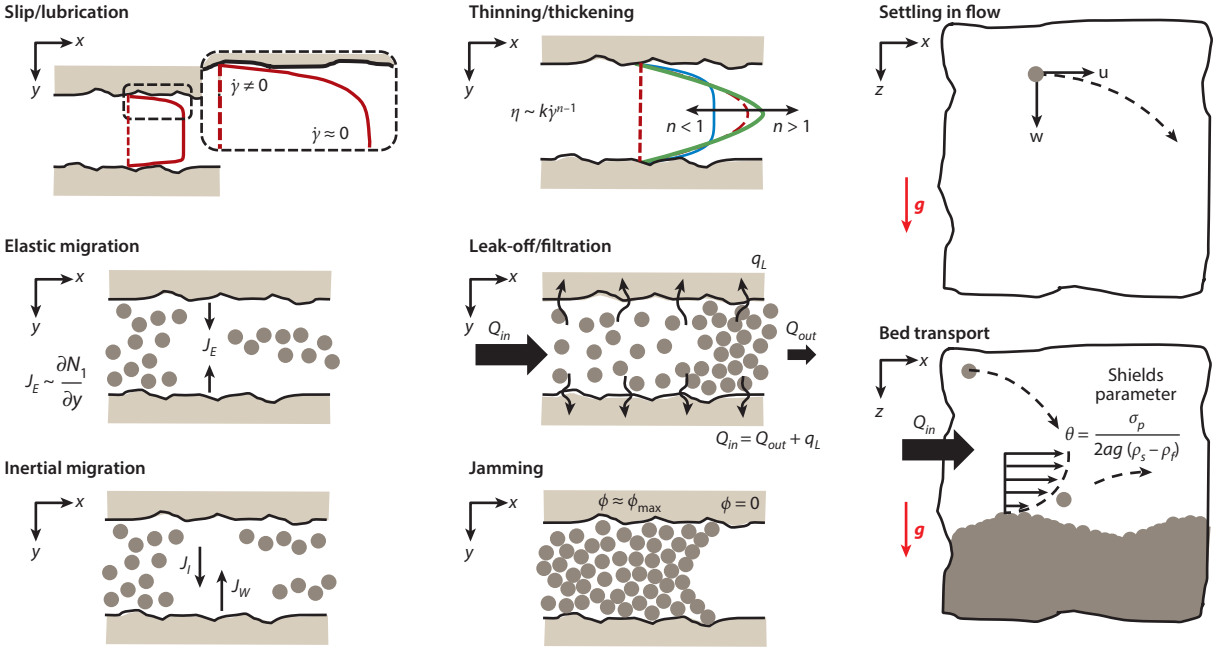

Figure 2

Schematic diagram of the fracturing process (*above*) and various transport phenomena involved in hydraulic fracturing. In the Shields parameter σ_p is the stress exerted on the particle by the flow.

reaction, whereas the addition of organic molecules (ligands) that screen the crosslinking sites can delay it. Pressure also affects the rheology: A decrease of 70% was reported in the viscosity of 0.3wt% hydroxypropyl guar crosslinked with diboronic acid when pressure was increased from atmospheric to 10,000 psi (124). Water chemistry (pH and ion content) must also be monitored, as species like bicarbonate, phosphate, magnesium, iron, and silicate can affect the crosslink density and hydration state of the guar (115, 125).

Breaker: additive to degrade the fluid microstructure and reduce the viscosity

Screenout: growth of a jammed proppant pack obstructing the flow in the fracture

Guar is often injected with delayed crosslinker and a breaker to modify the fluid rheology away from surface equipment. Ideally, crosslinking would occur immediately before the fluid transits the perforation to the fracture for the following reasons: (*a*) Crosslinking in the wellbore subjects the fluid to high rates of shear (typically 500–1,500/s), and may irreversibly damage the crosslinked network. (*b*) Crosslinked guar is more viscous and more difficult to pump, limiting the pumping rate (115). (*c*) Crosslinked guar more effectively carries proppant into the fracture, preventing sand from settling to the bottom of the pipe instead of entering the fracture. Even when crosslinking is delayed, the gel is exposed to extremely high shear rates in the jetlike flow through the perforation. Thus, the ability of the gel to heal and recover must be quantified to ensure that the desired rheological properties of the fluid are retained in the fracture. The breaker is added to degrade the guar (crosslinked or uncrosslinked) once the fracture has closed (115). Degradation is necessary to ensure that the ultimate conductivity of the fracture is not hindered by the presence of a viscous fluid or residual polymer. Oxidizers and enzymes (such as β-mannanase) can be used to cleave the acetyl linkages connecting mannose–mannose and mannose–galactose groups (105, 126).

Viscoelastic Surfactant-Based Fluids

Micellar surfactants in water constitute the so-called viscoelastic surfactant (VES) class of fluids. Introduced because of simplicity in design, preparation, and breaking requirements, the rheology of VES can be tuned by varying the surfactant concentration and the amount and type of salt or co-surfactant added to water. Because the surfactant molecules are amphiphilic and relatively short chained (as compared with polysaccharides), these fluids do not require time to hydrate and generally build structure rapidly upon addition to water. Above the critical micelle concentration, the VES forms long, wormlike structures that continuously break and reform, endowing the fluid with a Maxwell-like viscoelastic response (127). This microstructure is perturbed and the fluid thins when flowing through the perforation (high-shear region). Because the proppant-carrying ability depends critically upon the viscosity, the crucial design parameter is the fluid rehealing time versus the proppant settling time in the near-perforation region. If the fluid does not recover sufficiently quickly, the proppant will settle, accumulate, and occlude the perforation, resulting in screenout. The micellar fluid rheology is also strongly temperature sensitive; VES are typically used only in formations below 115°C.

VES has additional benefits: A breaker is not required when the formation contains mobile water, as VES can be broken by dilution with water (114). Permeability damage is reduced in the formation and proppant pack, as the surfactant micelles can dissolve in both aqueous and organic liquids. The strain-hardening extensional viscosity of VES reduces leak-off in formations with small pores. Furthermore, the rheology of such systems can be tuned such that the very high shear rate rheology translates into low frictional pressure losses in the pipe (in the turbulent regime). Purportedly owing to their strong elastic character, micellar fluids are recognized within the industry to transport proppant more effectively than Newtonian fluids with the same viscosity at identical flow conditions in the fracture. The main disadvantage, however, is the low pressure drop they create in the fracture (related to their shear banding). To remediate this issue and ensure

enough fracture aperture for proppant placement, VES are generally foamed. Although much is known about unladen VES, the current body of knowledge has not enabled a clear link between the structure of the surfactant and the resulting properties of the slurry, limiting the development of this family of fluids.

Energized Fluids, Foams, and Emulsions

All of the fluids described above can be energized (foamed) with nitrogen and/or carbon dioxide, and can also be added as inclusions in an immiscible organic fluid to build an emulsion (15, 114). Energized fluids and foams have the advantage of reduced water usage, while maintaining proppant transport ability. Furthermore, energized fluids require little or no breaker (the foam life can be controlled by surfactant chemistry) and tend not to damage the formation because a majority of the material (by volume) pumped downhole is gas and not water or oil (115). The rheology of foams and emulsions can be tuned through the fraction of the various phases, distribution of the size of the dispersed phase, and the interfacial tensions of the phases (108). Foams can exhibit viscosities far greater than the liquid phase and can exhibit a yield stress (128); they thus suspend proppant adequately, provide enough viscosity to create fracture width, and can provide adequate leak-off control.

Temperature and pressure variations from the surface to the fracture tip yield changes in the rheology of the foam and changes in the overall gas volume fraction. Foams must be designed to accommodate these changes, requiring interrogation at variable temperature, pressure, and mechanical stimuli. These materials are difficult to characterize in the lab, chiefly owing to slip and related artifacts (128, 129). Furthermore, the structure of foams, although shown to strongly control flow properties in both straight channels and porous media, is difficult to replicate in the laboratory.

Foams have been used historically to decrease the hydrostatic pressure in the wellbore, enabling hydraulic fracturing treatments in depleted reservoirs (with low reservoir fluid pressure and low reservoir stress). Despite strong potential benefits in reservoirs generally, the use of foams remains restricted to lower-pressure regions and low-volume treatments. Fluid selection is (again) mainly based on empirical experience, largely because of the lack of systematic understanding noted above. More recently, liquefied gas has been used as the liquid phase (to decrease formation damage) (130, 131), but this approach has not yet been comprehensively developed.

Slickwater and Waterfracs

The simplest materials used in hydraulic fracturing are the slickwater/waterfrac fluids. These materials target very-low-permeability reservoirs, where leak-off is minimal and generation of fracture surface area is paramount (132). These fluids are dilute polymer solutions [usually polyacrylamide (15) or propylene oxide] in which the polymer acts as a friction reducer (133) in the pipe, and not a viscosifier. Salts, clay-control additives (to mitigate clay swelling and permeability reduction), and other components may be added in small amounts (106). Mitigating pumping losses is a key issue, as these fluids are pumped at high rates to treat multiple fractures at once (upward of 120 bbl/min for 4 to 6 concurrent hydraulic fractures). Of all the fracturing fluids, proppant settling occurs most rapidly in slickwater. Because the carrying ability of these fluids is minimal, proppant concentrations $0 \leq \phi \lesssim 0.07$ are typically used.

The main advantage of slickwater fluids is their low cost, which has enabled economical production of unconventional reservoirs in North America. The main drawbacks are the minimal proppant-carrying ability, minimal fracture width generated, and challenges in fracture containment. Slickwater has been used recently in hybrid jobs, where slickwater is first pumped

to create narrow fractures in a complex network and is followed by a more viscous fluid to widen the fractures and carry higher concentrations of proppant (134). As with other fluids, the design of slickwater and hybrid jobs is largely guided by experience, even if fully numerical models are used to help with the design.

Fiber-Endowed Fluids

Fiber-endowed fracturing fluids are a relatively recent innovation, developed to improve proppant transport (135). Benefits of fiber-endowed fluids lie in their ability to partially decouple proppant transport ability from the base fluid rheology. This enables independent control of viscosity to achieve fracture width and fracture containment. The addition of fibers is particularly useful for high-temperature applications, where maintaining the fluid viscosity with chemical modifiers can prove difficult. Furthermore, fibers strongly reduce the effect of proppant diffusion during transport, both in the pipe and in the fracture. This ensures that the schedule of proppant concentration imposed at the surface is preserved along the wellbore and into the fracture. Specifically, this feature permits the pulsing of proppant-laden slugs with particle-free fluid, enhancing the post-treatment fracture conductivity.

Despite the success and wide use of fiber-endowed fluids, fundamental understanding of these systems is scant. This knowledge gap is likely the largest among all commonly used fracturing fluids. System design is complex, but based on experience at the lab- and field-scale, adequate systems typically consist of a polysaccharide (guar) base fluid, flexible fibers in the semidilute to concentrated regime, and proppant. The properties of these systems have not been comprehensively studied in the literature. Typically, simpler canonical systems have been studied, focusing on rigid fibers in Newtonian matrix fluids, in the absence of other solid particles (i.e., proppant).

The Need for Measurements

Fracturing fluids operate at high shear, high temperature, and high pressure; are laden with dense particles and potentially long, flexible fibers; and can be foamed. In isolation, each of these presents challenges. In conjunction, the experimental task is daunting. Regardless, measurement and theory are required to enable model-based fluid selection and design, rather than Edisonian approaches guided by empirical experience. Parametric exploration of the rheology of these materials, and measurements at high pressure and high temperature under both steady and dynamic forcing, would advance the field substantially.

COMPLEX FLUIDS IN HYDRAULIC FRACTURING

Fracturing fluid characterization is essential both for the design of new fracturing fluid systems and for the optimization of hydraulic fracturing treatments. It can be decomposed into two parts: The first goal is to provide an understanding of how (and if) the fluid answers the tremendously complex and often contradictory engineering requirements encountered in hydraulic fracturing. The second goal is to inform and validate fracturing and proppant transport models that are used to design and optimize hydraulic fracturing treatments. Tests associated with these goals should be standard protocols, as they need to be repeated for any new fluid formulation and (ideally) before any new fracture design. Such standard tests should be guided by the knowledge developed in the former, more detailed characterization. In this section, we consider the rheology of the base fluids (that also constitute the pad) and that of the particle-laden fluids (slurries).

Propping the fracture is an essential outcome of the hydraulic fracturing treatment. In addition to initiating and propagating the fracture, the fracturing fluid must transport and enable an even

distribution of particles to the instant of fracture closure. Avoidance of particle settling is thus a major consideration in particle transport—settling results in inhomogeneous placement along the length and height of the fracture and can cause the fracture to close in a wedge-like shape (136). Transported particles must navigate the vertical and horizontal wellbore, the perforation, and the fracture width and height, as well as the bifurcations and tortuosity encountered along the fracture length; nearly every point along the flow path is an opportunity for occlusion by the proppant.

Rheology and Rheometry of Fracturing Fluids

The response of the fluid stress as a function of shear rate and temperature is an important input to fracturing models (76) to determine both the geometry of the fractures and the power required to pump fluids downhole. Most numerical codes model the slurry as a continuous fluid using a shear-thinning viscosity model (76). Oilfield operators argue that determining a precise fluid viscosity is unnecessary owing to the weak dependence of fracture dimensions on the viscosity, as described in the section Implications for Fracturing Fluids. Even as the viscosity strongly influences leak-off, knowledge of the exact value may not be paramount, as the necessary rock properties are often a priori unknown, and independent tests must be carried out to characterize leak-off. Critically, these tests should also reveal the importance of fluid rheology (e.g., shear thinning), which has a non-negligible influence on fracture dimensions and deserves further attention. The flow behavior of suspensions, however, is critical to optimize proppant transport, as described in the next section.

Complex fluids exhibiting a dependence of stress on shear rate only (absent material memory and strain dependence) are classified as generalized Newtonian fluids. We provide a set of commonly used constitutive laws governing these fluids in **Table 5**. Common fracturing fluids are also often viscoelastic in character, exhibiting normal stress differences, memory, and other effects. More accurate descriptions and fits can be obtained by viscoelastic equations of state like the Giesekus or Kaye-Bernstein-Kearsley-Zapas models accounting for memory and strain effects (107, 109, 137), but these models are more challenging to implement both analytically and computationally.

Fracturing fluid rheometry. The bespoke design of fracturing fluids, coupled with the absence of universally predictive structure–function relationships, necessitates the direct measurement of complex fluid properties. Rheometers are used to measure the stress response to well-defined shearing motions generating (*a*) steady applied rate or stress, (*b*) steady-state and transient response to oscillations in amplitude and frequency (capturing both linear and nonlinear viscoelastic material

Table 5 Expressions for viscosity as a function of shear rate and particle volume fraction in generalized Newtonian fluids

Model	Expression	Remarks
Newtonian	$\eta(\dot{\gamma}) \to \mu$	Constant viscosity
Power law	$\eta(\dot{\gamma}) = k\dot{\gamma}^{n-1}$	Easiest to implement
Carreau $\eta(\dot{\gamma} \to \infty) = \eta_\infty$, $\eta(\dot{\gamma} \to 0) = \eta_0$	$\frac{\eta(\dot{\gamma}) - \eta_\infty}{\eta_0 - \eta_\infty} = (1 + (\lambda\dot{\gamma})^2)^{\frac{n-1}{2}}$	Captures low/high shear plateau and power law thinning at intermediate rates
Bingham ($n, k = \mu$), Herschel-Bulkley ($n \neq 1, k$ consistency)	$\frac{\eta}{\eta_0} = \begin{cases} \infty & \tau \leq \tau_y \\ k\dot{\gamma}^{n-1} + \frac{\tau_y}{\eta_0\dot{\gamma}} & \tau > \tau_y \end{cases}$	Thinning above τ_y; finite yield stress and shear thinning
Krieger-Dougherty	$\eta(\phi) = \eta_s \left(1 - \frac{\phi}{\phi_{\max}}\right)^{-[\eta]\phi_{\max}}$	η_s is the solvent phase viscosity ($\phi \to 0$)

response), and (*c*) start-up and cessation of stress or strain. Pressure-driven flows through slits, pipes, and constrictions can also be used to measure properties of pure fluids and suspensions under kinematic conditions closer to those downhole. Fewer commercial instruments exist to probe the extensional properties of complex fluids (useful for flow through perforations and porous media), with most being custom built (138). This is mainly due to difficulties in eliminating no-slip boundary conditions and in controlling the kinematics and flow strength (139).

Rheometric tests quantify several material functions: the shear viscosity $\eta(\dot{\gamma})$, normal stress differences $N_1(\dot{\gamma})$ and $N_2(\dot{\gamma})$, viscoelastic storage and loss moduli in response to imposed oscillations (at frequency ω and amplitude γ_0) $G'(\gamma_0, \omega)$ and $G''(\gamma_0, \omega)$, compliance $J(t)$, relaxation modulus $G(t)$, extensional viscosity $\eta_E(\dot{\gamma})$, and CaBER relaxation time (140), among others (107, 141). Measures of linear viscoelasticity are relatively well-defined and can be reproduced across different techniques, whereas numerous alternate measures of nonlinear viscoelasticity can be made and are often chosen to closely mimic the process that the data will inform.

Despite the availability of commercial fluids-characterization tools, care must be taken to properly execute experiments and interpret results. Several effects, generic to all complex fluids, are present and should be anticipated when performing experiments:

- Slip and shear banding. Slip, adhesive failure, and shear banding on the measuring instrument will compromise results. Unavoidable in many cases, they can be quantified with direct measurement (142) or inferred by repeated measurements varying the gap between parallel plates (129).
- Instabilities. Strongly viscoelastic fluids can exhibit spurious shear thickening owing to elastic (141, 143) or inertial instabilities (141). Predictive theories for the onset of instabilities are available in most geometries (113, 141) as a function of material properties and experiment parameters.
- Particle migration. Gradients in shear rate and elastic stress and nonzero streamline curvature promote particle migration; most rheometric shear flows have circular streamlines. The measurement time should be short as compared with the timescale for particle migration.
- Boundary effects. In addition to slip, rheometer boundaries can induce ordering and disturb the orientation of nonspherical particles (144). The geometry should be large as compared with the particle size, typically greater than 10 particle diameters (141).
- Measurement at elevated temperature and pressure. Reproducing downhole temperature and pressure introduces problems in sample drying and containment and is generally available only for steady measurements above 100°C (transient and dynamic measurements are challenging).
- Repeatability and mixing. Care must be taken to properly hydrate and mix additives in fluids (145), and also to ensure that the materials have not degraded or biologically decomposed when used over several days. In all cases the material should reflect the state of hydration/homogeneity used in the actual process.

In addition to shear, pressure-driven, and extensional rheometry, simpler index-based measures of rheological properties are also used (141). Common outside of academic laboratories, indicial measurements provide a simple diagnostic metric corresponding to pressure drop or torque in response to a poorly defined flow field. They are difficult to connect to models and microstructural material theories. Such indices are useful, however, in that they can provide rough quality-control checks that the target fluid will answer all requirements adequately. Common examples include friction factor–Reynolds number correlations and relative recovery of viscosity following extreme shear (15). These measures do not connect the microstructure of the fluid to its rheological properties.

Rheology of particle-laden fluids. Proppants are transported to the fracture to maintain conductivity after cessation of the flow/pressure from the surface. Proppants are classified by their strength (i.e., how much fracture-closure stress the proppant pack can sustain), average grain size and statistical distribution, the quantity of fines (that may reduce the pack permeability), roundness and sphericity, and density. Sand is commonly used, as are other materials, like resin- or polymer-coated particles, ceramics, or carbides, and hollow glass spheres may be added as proppants or as components in a mixture. As mentioned in the section on Fracturing Fluids, fibers are also added, not as proppant per se, but to modify fluid rheology and decrease settling rates (135), although fibers can also mechanically bridge the fracture. At the pump, the volume fraction (vol/vol) of the flowing suspension can range from 0% to 5% for waterfrac/slickwater applications (146), and to upward of 20% in treatments using more viscous fluids (147); these values increase along the fracture owing to leak-off. The size of the proppant particles used is guided by the expected width of the fracture during pumping and proppant concentration by the desired width during production, which is directly linked to the final amount of proppant per fracture area after closure. Particle size is specified by using the mesh size of a sieve; larger mesh values correspond to smaller particles. A 40/70 mesh sand is commonly used, corresponding to particles with approximate diameters between 210 μm and 420 μm.

Addition of particles will thicken the fluid owing to the additional viscous dissipation that arises at the no-slip boundary of each particle. This effect is well-characterized in Newtonian fluids and has been worked out to first order by Einstein and to second order by Batchelor: $\eta/\eta_s = 1 + \frac{5}{2}\phi + C_2\phi^2$. The constant C_2 depends on the flow type and the Péclet number (103, 148). At larger concentrations, no analytical solution is known; several empirical fits to data for monodisperse suspensions of spheres exist (102, 148), typically of the form given by the Krieger-Dougherty equation (**Table 5**), where ϕ_{max} is the maximum packing fraction for spheres in the suspension and $[\eta]$ is the specific viscosity (a function of particle shape), with $[\eta]\phi_{max} \approx 1.6$ for spheres. The viscosity diverges at ϕ_{max} and is very sensitive to small changes in particle concentration, except for small values of ϕ/ϕ_{max}.

Similar results follow for multimodal suspensions (149, 150). Chang & Powell (150) review and study the rheology of bimodal suspensions of spherical particles; at an identical total volume fraction, the viscosity of a bimodal suspension is lower than that of a monodisperse suspension, and this difference grows as the mismatch between particle sizes becomes larger. The same result follows for multimodal suspensions, as described by Farris (149), for whom the effect is named. This result is significant for fracturing—solids loading can be increased without sacrificing pumping power by selectively controlling the size distribution—provided the permeability of the proppant pack is preserved (151).

The dynamics of a fiber are drastically different than for spheres, even in the dilute limit. Jeffery (152) solved for the motion of an isolated, axisymmetric ellipsoid in a shear flow, demonstrating that particles orbit and sweep out a volume dependent upon the initial orientation of the ellipsoid. Rigid fibers fit well into this framework—they can be modeled as ellipsoids where the aspect ratio $r_p = \frac{\text{major axis}}{\text{minor axis}} = \frac{L}{d} \gg 1$. Suspensions of fibers may be classified according to the nature of interactions among the fibers (144). Suspensions are considered dilute when the distance between fiber centers avoids contact and hydrodynamic interactions are negligible ($>L$), satisfied when $\phi \lesssim r_p^{-2}$. Incorporating hydrodynamic interactions with minimal particle–particle contacts establishes the semidilute window, $r_p^{-2} \lesssim \phi \lesssim r_p^{-1}$; everything above this window ($\phi > r_p^{-1}$) is considered the concentrated regime, in which interactions between fibers contribute strongly to the fluid rheology.

In the dilute regime, fibers viscosify the fluid less than spheres at the same volume fraction, as they spend most of their existence aligned with the flow during their Jeffery orbit. This is

communicated quantitatively through the specific viscosity of fiber suspensions (ellipsoids with $r_p \to \infty$), found by Jeffery to be $[\eta] = 2$; similar results have been computed by many others [see table 1 in Petrie's review on fiber suspension rheology (153)]. In the semidilute regime, for the same solids concentration, suspensions with larger r_p will exhibit a larger viscosity (154). The aspect ratio and concentration are not the only controlling parameters, however, as the fiber length has been shown to influence the viscosity for fixed r_p and ϕ (154); this length effect is presumably due to the presence of flocs formed by adhesive contacts and between the particles and is mitigated at large stresses (155). Other effects, like the orientation and buckling of fibers, contribute strongly to suspension rheology and stress growth in the start-up of shear flows.

The volume fraction required to form a mechanical contact network (ϕ_c) decreases strongly as the particle becomes less spherical (156), scaling as $\phi_c \sim 0.6 r_p^{-1}$ to lowest order in the aspect ratio for prolate ellipsoids. This suggests that mechanically connected networks of fibers can be formed at smaller volume fractions as compared with spheres, where $\phi_c \sim 0.28$ (156). This result has been exploited in fiber-endowed fracturing fluids (135).

Shear thickening is also observed in some fracturing fluids. Particle-laden flows will exhibit an increase of viscosity with increasing shear rate provided the suspension is above approximately 40% solid particles; the magnitude of shear thickening becomes increasingly severe as the concentration of particles increases (102, 157). The shear thickening described here is dynamic and distinct from the viscosity enhancement that arises from simply adding particles to a fluid (where no slip on the particle surfaces enhances the local viscous dissipation rate as the volume fraction of the solid phase increases). Recent reviews by Denn & Morris (158) and Stickel & Powell (148) and monographs by Guazzelli & Morris (103) and Mewis & Wagner (102) provide extensive discussion of suspension rheology and mechanics for non-Brownian particles.

Describing the rheology of filled non-Newtonian liquids is significantly more complex owing to the variety of fluid behaviors and constitutive laws available—experiments and theory required to classify and describe each are extensive and difficult. Barnes (159) provides a recent review of particulate suspensions in non-Newtonian fluids. Although generalized statements are difficult to justify for particles in non-Newtonian matrix fluids, many viscoelastic particle-laden systems display a magnification of viscoelastic effects in the fluid phase owing to the increased local shear rate resulting from the presence of solids. Gleissle and coworkers (160, 161) explored this effect, showing that a shift factor dependent on volume fraction can accurately predict material functions of many particle–fluid systems. Dagois-Bohy et al. (162) have recently explored the non-Newtonian rheology of a suspension in a yield-stress fluid and showed that extension of Newtonian results to these fluids is promising but nontrivial.

Particle Migration

The oilfield community started to investigate particle migration under fluid flow in the late 1980s (163). There was a concern that settling would be accelerated if particles migrated to the center of the fracture width, both under flow and at rest. Another concern is the increased velocity of the particles in the fracture midplane, which may reach the tip of the fracture and cause bridging (164). Particle migration arises from several forces present in both Newtonian and non-Newtonian fluids.

Segré & Silberberg (165, 166) studied the migration of a dilute suspension of particles in low–Reynolds number flow of Newtonian fluids, observing particle concentration at approximately 60% of the tube radius. Theory applied to migration in this dilute limit generally agrees with experiment (167, 168), revealing that a balance between an inertial lift force and a repulsion near the wall is responsible for the equilibrium distribution. At higher Reynolds numbers, the concentrate annulus moves toward the wall. Matas et al. (169) characterize this behavior for $67 \leq \mathrm{Re} \leq 2{,}400$

and observe a second equilibrium position at the tube center when $\mathrm{Re} \geq 600$, which is also a function of particle size. Asmolov (170) provides a theoretical description of particle migration in this limit but does not predict the second equilibrium region.

Non-dilute suspensions under flow exhibit particle migration owing to gradients in viscosity, shear rate, and particle concentration. Acrivos and coworkers (171, 172) observed these effects in the rheometry of suspensions, where particles migrated to regions of low shear rate in a Couette cell. Similar effects have been observed in duct flows of suspensions (173, 174), showing the transport of particles toward the channel centerline and a blunting of the velocity profile with increasing volume fraction. Oh et al. (175) determined that the center region could reach $\phi = 0.64$, the random close packing limit of monodisperse spheres, demonstrating that these domains progressively compact.

The driving mechanisms are well-described in constitutive models by Phillips et al. (176) and Mills & Snabre (177). Phillips et al. (176) use a diffusive flux approach, in which particle concentration plays the role of an active scalar that diffuses as a result of several gradient terms. Particles migrate away from regions of high collision frequency, corresponding to regions of large shear and/or particle concentration, $J_{p-p} \sim -\nabla(\dot{\gamma}\phi)$. Further, particles migrate away from regions of large viscosity; a colliding particle pair in a region of inhomogeneous ϕ [and therefore $\eta(\phi)$] will exhibit a net displacement toward the region of lower viscosity, $J_\eta \sim -\nabla(\eta(\phi))$. Mills & Snabre (177) predict migration based upon gradients in the stress [rather than upon local particle collision rates as considered by Phillips et al. (176)]. Recent analyses (178, 179) employ the frictional rheology model of Boyer et al. (180). Both capture the migration of particles toward the center and resultant blunting of the parabolic flow profile. The distribution of particles has been measured (175) and demonstrates the applicability of these models (178, 180).

In viscoelastic fluids, migration can also occur due to an elastic force orthogonal to the direction of shearing. Elastic (normal) forces are largest in regions of large shear rate; gradients in the shear rate across a particle will result in a net elastic force pushing particles to regions where the gradient in shear rate—and resulting elastic stress gradient—is small. In a Poiseuille flow, particles therefore migrate toward the apex of the velocity profile. This effect has been described in a second-order fluid by Ho & Leal (110) and experimentally verified by Tehrani (181). Leshansky et al. (111) performed experiments showing particle focusing in a microdevice and derived a scaling argument identical to Tehrani's for the migration speed, $v \sim -\frac{a^2}{6\pi\eta}\frac{\partial N_1}{\partial \dot{\gamma}}\frac{\partial \dot{\gamma}}{\partial y}$, where N_1 is the first normal stress difference and y is the cross-channel dimension. Tehrani also illustrated the importance of the shear rate, observing the absence of particle migration in the plug-flow region of an elastic solution.

Elastic forces also give rise to subtle and surprising particle–particle interactions. Feng & Joseph (182) studied these interaction effects in torsional shearing flow between parallel plates, observing the formation of annular rings using both spheres and fibers in a polyox solution; interestingly, fibers can rotate inward or outward depending on whether the fiber is free to rotate about the vorticity axis or is stuck in a state aligned with the flow. Lim et al. (183) explored these effects in rigid microfluidic devices at high Reynolds number. Iso, Koch & Cohen (184, 185) studied semidilute concentrations of fibers in fluids of varying elasticity in a Couette flow and highlighted the competition between particle–particle hydrodynamic interactions and elasticity-driven fluid effects. Fibers tend to align toward the vorticity axis in weakly elastic fluids ($Wi \ll 1$, log rolling) but become increasingly randomized when the fiber concentration increases, whereas fibers tend to align in fixed orientations (along and slightly offset from flow) in strongly elastic fluids [$Wi \gtrsim O(1)$].

The nature of the non-Newtonian fluid determines the nature of the particle–particle interactions. In a study of particle–particle interactions in a shear flow, Snijkers et al. (186) detailed these differences in both the rheology of the fluid and resulting particle trajectories. A

unifying theme of elastic fluids, however, is the tendency to exert an inward compressive force normal to curved streamlines, which can explain particle–particle kissing, streamwise orientation of elongated particles, and particle motion toward walls (187). An improved understanding of these effects may provide insight into the trajectory of proppants in a complex network of fractures, e.g., which components of a proppant will effectively move from the main fracture into an adjacent fracture, making a sharp angle with it.

Particle Settling

Proppant settling occurs under both dynamic (during flow) and static conditions. Elimination and mitigation of settling are important to ensure a uniform distribution of proppant particles along a fracture; settling will occur unless the proppant and fluid are density matched. The presence of boundaries, non-Newtonian base fluids, and other particles all modify the settling of proppants within a fracture.

Two distinct regimes of settling behavior are recognized to exist during the fracturing process: (*a*) rapid settling coupled with successive rolling, saltation, and resuspension of the sediment bed and (*b*) gradual settling absent a moving sediment bed. In all cases, descriptions of particle transport are dominated by empirical correlations, except where exact zero Reynolds number results can be applied (188). In 1959, Kern et al. (189) recognized the sediment transport described in the first regime. The relevant physical parameters are the shear stress acting on the grain compared with a gravitational stress, $\theta = \frac{\tau_p}{2ag(\rho_s - \rho_f)}$ (the Shields parameter), and the particle Reynolds number $\mathrm{Re}_p = \frac{\rho_f a w \dot{\gamma}}{\eta}$. Sediment transport is anticipated in waterfrac/slickwater operations (190), the onset of which can be predicted using a Shields plot (191). This process, specific to the fracturing configuration, was studied in more detail by Patankar et al. (192) and Wang et al. (193), who developed power law correlations to describe static and fluidized bed heights in a fracture.

Proppant particles in more concentrated polymer and gel-like fluids will experience reduced settling, owing to the enhanced viscosity of the fluid. Sedimenting particles experience frictional drag and a variety of particle- and wall-driven retarding phenomena prior to deposition in a pack on the bottom of the fracture. The convecting particles experience all of the migration forces described above, and additionally feel a gravitational body force. This body force drives particles downward to the fracture floor; conservation of mass and the migration of neighboring particles drive a recirculation (103), which retards the settling speed. A result by Richardson & Zaki (103, 194), $u = u_s(1 - \phi)^{-n}$, predicts the decrease in the Stokes settling speed, u_s, as a function of volume fraction, ϕ. The power-law exponent $n \approx 5$ is determined empirically (103, 195). In this expression, the volume fraction is uncorrected for maximum packing and will lose predictive capability at higher particle concentrations; Chang & Powell (196) introduce a modified version of this law to correct for the maximum packing limit, $u = u_s(1 - 0.05\phi/\phi_{\max})^{5.3\pm0.2}$.

Particles sediment differently under both static and flowing conditions when embedded in non-Newtonian fluids (**Figure 3**). This aspect of fracturing fluids has been studied in the petroleum industry since at least the 1970s. Some efforts have focused on the development of empirical correlations to predict settling of particles in shear-thinning or Carreau-like fluids (188, 197, 198), whereas others have tackled the static versus dynamic settling problem directly. Novotny (199) performed experiments in a Couette cell using a polyacrylamide fluid and observed enhanced settling when the suspension was sheared, even remarking that particles that appeared to be completely stagnant in a "highly non-Newtonian fluid" will sediment once sheared. McMechan & Shah (200) studied the static settling of particles in a 14-ft-tall cell using a variety of metal and borate crosslinked guar fluids and remarked on the suspending ability of the various crosslinkers.

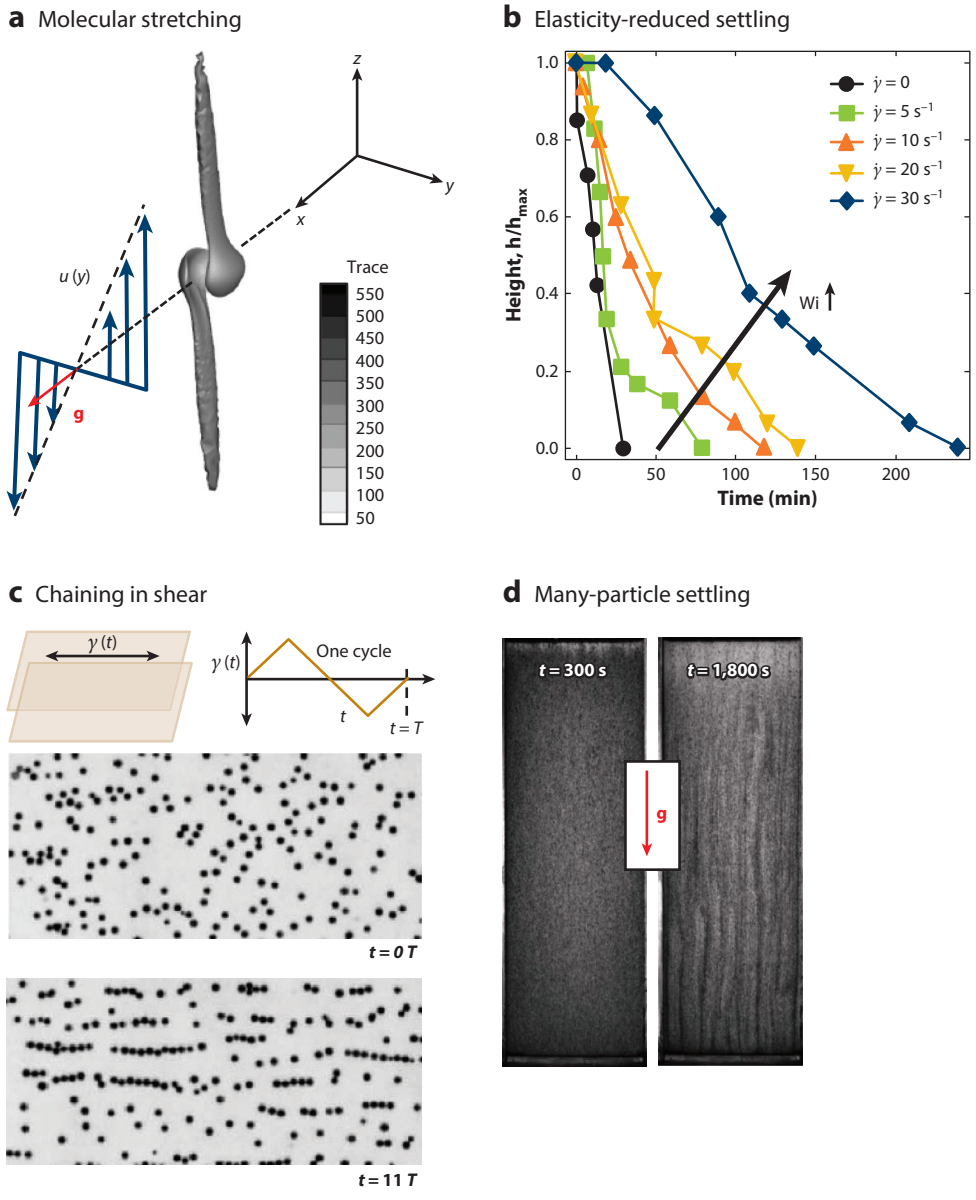

Figure 3

Single- and many-particle effects under settling and shear. (*a*) Trace of the conformation tensor surrounding a settling particle under shear (201) illustrating regions of pronounced molecular stretching length and regions of elastic stress (reprinted from Reference 201, ©2013, with permission from Elsevier). (*b*) Settling of particles through a stationary ($\dot{\gamma} = 0$) and sheared fluid [reprinted with permission from Tonmukayakul et al. (202) ©2008, AIP Publ. LLC] illustrating increased drag on a settling suspension when $\dot{\gamma} > 0$. Many-particle interactions induce particle chaining and fluid channeling from a homogenous state (*c*) in a periodic triangle wave Couette flow (203) (reprinted from Reference 203, ©2004, with permission from Elsevier) and (*d*) under settling (204) (reprinted figure with permission from Reference 204, ©2005 Am. Phys. Soc.).

In particular, they noted variability in the time for the proppant-carrying capacity of the materials to recover following pumping and shearing to fill the cell.

Extensive experiments using Couette and slit-flow geometries indicate that fluid elasticity is required to retard settling in dynamic conditions, and that the microstructure of the non-Newtonian fluid and shear conditions are essential to determine the ability of the fluid to retard (or enhance) settling under dynamic conditions. Gheissary & van den Brule (205, 206) studied Newtonian, constant-viscosity elastic fluids (i.e., Boger fluids) and a viscoelastic shear-thinning fluid. They found that settling is retarded in the Boger and viscoelastic shear-thinning fluids, with the highest-elasticity fluid (as measured by the first normal stress difference) giving the slowest settling rates, even if the fluid shear-thins. They also commented on flow-induced anisotropy: Flow of fluids that shear-thin owing to alignment of polymer molecules (hydroxyethyl cellulose, for example) will exhibit slower settling than shear-thinning fluids that decrease their viscosity as a result of the breakdown in the internal microstructure (such as Carbopol). Tonmukayakul et al. (202) tuned the amount of borate crosslinker in a guar gum solution and showed that at lower crosslinker concentration (corresponding to a weakly elastic, shear-thinning fluid), the settling rate increases with shear rate, whereas at higher crosslinker concentration (a viscoelastic gel-like fluid), the settling rate markedly decreases with shear rate. The experiments by Hu et al. (207–209) focus on differences between borate and metal crosslinked guars, with high-concentration crosslinkers. Microstructurally, these materials differ in the nature of the crosslinks: Addition of borate introduces dynamic crosslinks, enabling the material to reheal following breaking (119, 120), whereas the metal-based crosslinks are irreversible and do not reform once broken (115, 123). Settling in each gel under shear then proceeds differently. Settling in the borate crosslinked guar is retarded by imposed crossflow, and both N_1 and η increase as a result of shear. Conversely, minimal settling is observed in metal crosslinked gels at low or zero shear rates, but above a critical shear rate, the proppant-carrying ability of the material is lost, and substantial settling is observed.

The retarded settling of particles within non-Newtonian fluids subjected to shear flow has also been examined computationally and analytically. Tanner, Housiadas, and coworkers (210, 211) have studied the drag on a sphere, pointing to an added elastic stress contributed by the distortion of streamlines induced by the settling particle. Padhy et al. (201, 212) performed computations using FENE-P and Giesekus models to mimic a Boger fluid and a guar solution lightly crosslinked with borate [which shows enhanced settling with increasing shear rate in experiments (202)]. Their computations captured the retarded settling observed in experiments and also captured the result of Housiadas & Tanner (210) when walls bounding the flow are removed (infinite domain). Padhy et al. (201, 212) examined individual contributions to the total drag and highlighted the competition between elasticity (which increases frictional drag) and shear thinning (which decreases drag). They further noted that these phenomena scale differently with polymer concentration, and an optimum concentration exists to minimize the sedimentation speed (212).

The complexity of the nonlinear transport phenomena presented here, compounded with complex temperature, pressure, and shear-rate history experienced by a slurry during a hydraulic fracturing treatment, yields very conservative assumptions in the design and optimization of hydraulic fracturing treatments. For example, settling rates are typically overestimated to make sure that the design will result in an acceptable distribution of proppant in the fracture. Acceptable fracture extensions are then limited as a result, to make sure that proppant does not settle at the bottom of the fracture.

Bridging and Jamming Events

Proppant occasionally becomes stuck, or jammed, during fluid injection. This event is known to occur both in the immediate vicinity of the wellbore and close to the fracture tip. In narrow

Jam: a particle pack in the fracture with enhanced hydraulic resistance accumulating proppant but permitting fluid to filter through

Bridge: a fracture-spanning group of stuck particles, around which other particles and fluid may flow

apertures, jamming events may start after the formation of a localized force chain or bridge of particles between the fracture walls. Bridged proppant will redirect the local flow around it and may either become destabilized (unbridged) or grow. Under continuous pumping of slurry, the jammed proppant pack may grow, creating a region of locally magnified resistance, until the fracture and the wellbore are filled with proppant—or pumping is stopped. The pressure at the surface can increase rapidly during jamming and may reach the maximum pressure capacity of the equipment. Growth of a jammed pack, termed a screenout, constitutes failure if it prevents completion of the treatment, especially when it happens in the near wellbore, as it halts the fracturing job and requires well cleaning. On the contrary, a screenout can be planned to happen further down the fracture, ideally with limited pad left if the fracture design is perfect, stopping the fracture from growing and allowing more packing of the fracture with proppant than would be possible without this event taking place (tip-screenout technique). A myriad of particle migration mechanisms have been implicated, along with fluid-phase leak-off, in suspension flow, bridging, jamming, and tip screenout in the fracturing process. Chekhonin & Levonyan (213) consider suspension flow in a KGD fracture to establish parameters for tip screenout, computationally modeling the suspension concentration along the fracture length only and dividing the flow into regions that are Poiseuille–like ($\phi < \phi_{max}$) or Darcy–like ($\phi = \phi_{max}$). Dontsov & Peirce (214, 215) consider both KGD and pseudo-3D fracture models using a frictional rheology model incorporating slip and settling within a fracture. These results confirm that proppant screenout (owing to leak-off-driven concentration and settling) can drive strong changes in fracture geometry, which was established in industry through a combination of treatment monitoring and simpler modelling efforts.

Control and prediction of bridging and jamming are critical to avoid and program screenout. Jamming is predicted sufficiently well when solids reach a maximum volume fraction. As for bridging, fracture models typically predict bridging events when the ratio of slot width/particle size is below 3 to 10—a number that is tuned by experience but consistent with bridging studies in granular (216) and non-Brownian (217) systems, which reveal the stochastic nature of the process. The difficulty comes partially from the physics controlling the phenomena: Bridging is a discrete event governed by probabilities of occurrence that are not resolved by continuum models or accurately predicted by discrete models. The sphericity and frictional properties of the particle certainly play a role, and the pronounced effects such properties have on suspension rheology are now beginning to be considered (218). In addition to tip-screenout designs, the dramatic consequences of bridging/jamming have been advantageously applied in diversion techniques, where a fracture is locally jammed and the particle-laden fluid is redirected to stimulate other parts of the oilfield reservoir (219), or in the form of a fluid loss control additive, where operators want to locally eliminate leak-off to the formation (220).

CONCLUSIONS

Hydraulic fracturing, and hydrocarbon recovery operations in general, presents a grand challenge for non-Newtonian fluid dynamics. Complex fluids used in fracturing operations encompass essentially all aspects of rheology and non-Newtonian fluid dynamics—linear and nonlinear viscoelasticity, physicochemical gelation, transport and orientation of spherical and fibrous particles, control of slip/shear banding, and migratory and many-body particle interactions are present in abundance and intimately affect the ultimate hydrocarbon recovery that can be achieved. These manifold effects match the spectrum of specific fluids employed to target rock formations of widely varying permeability, porosity, mechanical properties, depth, and temperature. Understanding and integrating non-Newtonian fluid mechanics with reservoir

attributes and statistical variability is a key contributor to improved resource recovery and constitutes an intellectually rich and economically relevant research problem for years to come.

SUMMARY POINTS

1. Hydraulic fracturing is a key stimulation technique in hydrocarbon recovery, primarily targeting reservoirs of low intrinsic permeability.
2. Hydrocarbon reservoirs exhibit widely variable mechanical, chemical, and environmental properties.
3. Particle-laden complex fluids with a wide range of rheological characteristics are used to open and sustain hydraulic fractures.
4. Quantitative descriptions of non-Newtonian fluid mechanics are essential to predict complex fluid (and hence fracturing) performance.

FUTURE ISSUES

1. Improvement and development of constitutive (particularly nonlinear) models for physical gels and supramolecular systems to model crosslinked and associating complex fluids.
2. Mechanistic descriptions of particle–particle (both proppant and fiber) and particle–fluid interactions under pressure- (or shear-)driven flow with superposed gravitational settling.
3. Material property measurements under representative temperatures and pressures and shear rates to match downhole conditions.
4. Development of laboratory (milli- and microfluidic)-scale experiments quantifying reservoir–fluid–proppant interactions in flow regimes representative of hydraulic fracturing dynamics, geometry, and materials.
5. Creation of coupled, multiscale, time-dependent simulations capturing complex fluid rheology and particle transport during pumping, fracturing, leak-off, and fracture closure.

DISCLOSURE STATEMENT

The authors are not aware of any affiliations, memberships, funding, or financial holdings that might be perceived as affecting the objectivity of this review.

ACKNOWLEDGMENTS

We thank E.B. Dussan V. and Francois M. Auzerais for helpful and stimulating discussions.

LITERATURE CITED

1. Ingraffea AR, Wells MR, Santoro RL, Shonkoff BC. 2014. Assessment and risk analysis of casing and cement impairment in oil and gas wells in Pennsylvania, 2000–2012. *PNAS* 111:10955–60
2. Van Dyke JW. 1896. *Increasing the flow of oil-wells.* US Patent No. 556651
3. Thomas RL, Morgenthaler LN. 1999. Introduction to matrix treatments. In *Reservoir Stimulation*, ed. MJ Economides, KG Nolte, pp. 1–38. Hoboken, NJ: John Wiley & Sons

4. Frenier W, Ziauddin M. 2014. *Chemistry for Enhancing the Production of Oil and Gas.* Richardson, TX: Soc. Pet. Eng. 606 pp.
5. Grebe JJ, Stoesser SM. 1935. *Treatment of deep wells*. US Patent No. 1998756 A
6. Grebe JJ, Stoesser S. 1935. Increasing crude production 20,000,000 bbl. from established fields. *World Pet. J.* 6(8):473–82
7. Howard GC, Fast CR. 1970. *Hydraulic Fracturing*, Vol. 2, *Monograph (Society of Petroleum Engineers of AIME), Henry L. Doherty Series*. New York: Soc. Pet. Eng.
8. Gallegos TJ, Varela BA. 2015. *Trends in hydraulic fracturing distributions and treatment fluids, additives, proppants, and water volumes applied to wells drilled in the United States from 1947 through 2010—data analysis and comparison to the literature*. US Geol. Surv. Investig. Rep. 2014-5131
9. Ventura J. 2015. *Range Resources*. Presented at EnerCom Oil Gas Conf., Aug. 16–20, Denver, CO
10. Rice Energy. 2015. *2nd quarter 2015 supplemental slides.* Tech. Rep., Rice Energy
11. Corporation COG. 2015. *Cabot Oil and Gas Corporation.* Presented at EnerCom Oil Gas Conf., Aug. 16–20, Denver, CO
12. Chesapeake Energy. 2015. *2nd quarter earnings report*. Tech. Rep., Chesapeake Energy
13. Kennedy RL, Knecht WN, Georgi DT. 2012. *Comparisons and contrasts of shale gas and tight gas developments, North American experience and trends*. Presented at SPE Saudi Arabia Sect. Tech. Symp. Exhib., April 8–11, Al-Khobar, Saudi Arab.
14. Turcotte DL, Moores EM, Rundle J. 2014. Super fracking. *Phys. Today* 67:34–39
15. Montgomery C. 2013. Fracturing fluid components. In *Effective and Sustainable Hydraulic Fracturing*, ed. AP Bunger, J McLennan, R Jeffrey. Rijeka, Croat.: InTech
16. Selley RC. 1975. *An Introduction to Sedimentology*. Cambridge, MA: Academic
17. Dietrich RV, Skinner BJ. 1979. *Rocks and Rock Minerals*. Hoboken, NJ: John Wiley & Sons
18. Tiab D, Donaldson EC. 2012. *Petrophysics: Theory and Practice of Measuring Reservoir Rock and Fluid Transport Properties*. Houston: Gulf Prof. Publ.
19. Lee WHK, Uyeda S. 1965. Review of heat flow data. In *Terrestrial Heat Flow*, ed. WHK Lee, pp. 87–190. Washington, DC: Am. Geophys. Union
20. Tissot BP, Welte DH. 1984. *Petroleum Formation and Occurrence*. Berlin: Springer-Verlag
21. Dow WG. 1977. Kerogen studies and geological interpretations. *J. Geochem. Explor.* 7:79–99
22. Vandenbroucke M, Largeau C. 2007. Kerogen origin, evolution and structure. *Org. Geochem.* 38:719–833
23. McCarthy K, Rejas K, Niemann M, Palmowski D, Peters K, Stankiewicz A. 2011. Basic petroleum geochemistry for source rock evaluation. *Oilfield Rev.* 23:32–43
24. Soeder DJ. 1988. Porosity and permeability of eastern Devonian gas shale. *SPE Form. Eval.* 3:116–24
25. Neuzil CE. 1994. How permeable are clays and shales? *Water Resour. Res.* 30:145–50
26. Dewhurst DN, Yang Y, Aplin AC. 1999. Permeability and fluid flow in natural mudstones. *Geol. Soc. Lond. Spec. Publ.* 158:23–43
27. Dewhurst DN, Aplin AC, Sarda J-P, Yang Y. 1998. Compaction-driven evolution of porosity and permeability in natural mudstones: an experimental study. *J. Geophys. Res. Solid Earth* 103:651–61
28. Aplin AC, Matenaar IF, McCarty DK, van der Pluijm BA. 2006. Influence of mechanical compaction and clay mineral diagenesis on the microfabric and pore-scale properties of deep-water Gulf of Mexico mudstones. *Clays Clay Miner.* 54:500–14
29. Loucks RG, Reed RM, Ruppel SC, Hammes U. 2012. Spectrum of pore types and networks in mudrocks and a descriptive classification for matrix-related mudrock pores. *AAPG Bull.* 96:1070–98
30. Aydin A. 2000. Fractures, faults, and hydrocarbon entrapment, migration and flow. *Mar. Pet. Geol.* 17:797–814
31. Anders MH, Laubach SE, Scholz CH. 2014. Microfractures: a review. *J. Struct. Geol.* 69:377–94
32. Hooker JN, Laubach SE, Marrett R. 2014. A universal power-law scaling exponent for fracture apertures in sandstones. *GSA Bull.* 126:1340–62
33. Bernard S, Horsfield B. 2014. Thermal maturation of gas shale systems. *Annu. Rev. Earth Planet. Sci.* 42:635–51
34. Nelson PH. 2009. Pore-throat sizes in sandstones, tight sandstones, and shales. *AAPG Bull.* 93:329–40

35. Passey QR, Bohacs KM, Esch WL, Klimentidis R, Sinha S. 2010. From oil-prone source rock to gas-producing shale reservoir—geologic and petrophysical characterization of unconventional shale-gas reservoirs. *Proc. Int. Oil Gas Conf. Exhib. China, 8–10 June, Beijing, China*, SPE-131350-MS. Richardson, TX: Soc. Pet. Eng.
36. Bear J. 1972. *Dynamics of Fluids in Porous Media*. Mineola, NY: Dover
37. Scheidegger AE. 1974. *The Physics of Flow through Porous Media*. Toronto: Univ. Tor. Press
38. Koplik J, Levine H, Zee A. 1983. Viscosity renormalization in the Brinkman equation. *Phys. Fluids* 26:2864–70
39. Larson RG. 1981. Derivation of generalized Darcy equations for creeping flow in porous media. *Ind. Eng. Chem. Fundam.* 20:132–37
40. Pearson JRA, Tardy PMJ. 2002. Models for flow of non-Newtonian and complex fluid through porous media. *J. Non-Newton. Fluid Mech.* 102:447–73
41. Morais AF, Seybold H, Herrmann HJ, Andrade JS. 2009. Non-Newtonian fluid flow through three-dimensional disordered porous media. *Phys. Rev. Lett.* 103:194502
42. Klinkenberg LJ. 1941. *The permeability of porous media to liquids and gases*. Presented at Drill. Prod. Pract., Jan. 1, New York
43. Javadpour F. 2009. Nanopores and apparent permeability of gas flow in mudrocks (shales and siltstone). *J. Can. Pet. Technol.* 48:16–21
44. Darabi H, Ettehad A, Javadpour F, Sepehrnoori K. 2012. Gas flow in ultra-tight shale strata. *J. Fluid Mech.* 710:641–58
45. Katz AJ, Thompson AH. 1985. Fractal sandstone pores: implications for conductivity and pore formation. *Phys. Rev. Lett.* 54:1325–28
46. Katz AJ, Thompson AH. 1986. Quantitative prediction of permeability in porous rock. *Phys. Rev. B* 34:8179–81
47. Curtis JB. 2002. Fractured shale-gas systems. *AAPG Bull.* 86:1921–38
48. Gale JFW, Reed RM, Holder J. 2007. Natural fractures in the Barnett shale and their importance for hydraulic fracture treatments. *AAPG Bull.* 91:603–22
49. Gale JFW, Laubach SE, Olson JE, Eichhubl P, Fall A. 2014. Natural fractures in shale: a review and new observations. *AAPG Bull.* 98:2165–216
50. King GE. 2010. *Thirty years of gas shale fracturing: What have we learned?* Presented at SPE Annu. Tech. Conf. Exhib., Sept. 19–22, Florence, Italy
51. Berkowitz B. 2002. Characterizing flow and transport in fractured geological media: a review. *Adv. Water Resour.* 25:861–84
52. Sahimi M. 2011. *Flow and Transport in Porous Media and Fractured Rock*. Weinheim, Ger.: Wiley-VCH. 2nd ed.
53. Zimmerman RW, Bodvarsson GS. 1996. Hydraulic conductivity of rock fractures. *Transp. Porous Media* 23:1–30
54. Barenblatt GI, Zheltov IP, Kochina IN. 1960. Basic concepts in the theory of seepage of homogeneous liquids in fissured rocks [strata]. *J. Appl. Math. Mech.* 24:1286–303
55. Warren JE, Root PJ. 1963. The behavior of naturally fractured reservoirs. *Soc. Pet. Eng. J.* 3:245–55
56. Kuchuk F, Biryukov D. 2014. Pressure-transient behavior of continuously and discretely fractured reservoirs. *SPE Reserv. Eval. Eng.* 17:82–97
57. Lockner DA. 2013. Rock failure. In *Rock Physics & Phase Relations: A Handbook of Physical Constants*, ed. TJ Ahrens, pp. 127–47. Washington, DC: Am. Geophys. Union
58. Kohlstedt DL, Evans B, Mackwell SJ. 1995. Strength of the lithosphere: constraints imposed by laboratory experiments. *J. Geophys. Res.* 100:17587–602
59. Alford J, Blyth M, Tollefsen E, Crowe J, Loreto J, et al. 2012. Sonic logging while drilling—shear answers. *Oilfield Rev.* 24:4–15
60. King MS. 1969. *Static and dynamic elastic moduli of rocks under pressure*. Presented at 11th US Symp. Rock Mech., June 16–19, Berkeley, CA
61. Warpinski NR, Smith MB. 1989. Rock mechanics and fracture geometry. In *Recent Advances in Hydraulic Fracturing*, Vol. 12, *Henry L. Dougherty Series*, ed. JL Gidley, SA Holditch, DE Nierode, RW Veatch Jr., pp. 57–80. Richardson, TX: Soc. Pet. Eng.

62. Warpinski NR, Teufel LW. 1989. In-situ stresses in low-permeability, nonmarine rocks. *J. Pet. Technol.* 41:405–14
63. Senseny PE, Pfeifle TW. 1984. *Fracture toughness of sandstones and shales.* Presented at 25th US Symp. Rock Mech., June 25–27, Evanston, IL
64. Brown ET, Hoek E. 1978. Trends in relationships between measured in situ stresses and depth. *Int. J. Rock Mech. Min. Sci. Geomech. Abstr.* 15:211–15
65. Warpinski N. 2011. Fracture growth in layered and discontinuous media. In *Proceedings of the Technical Workshops for the Hydraulic Fracturing Study: Fate and Transport*. Washington, DC: Environ. Prot. Agency
66. Hubbert MK, Willis DG. 1957. Mechanics of hydraulic fracturing. *Pet. Trans.* 210:153–68
67. Teufel LW, Clark JA. 1984. Hydraulic fracture propagation in layered rock: experimental studies of fracture containment. *Soc. Pet. Eng. J.* 24(1):19–32
68. Warpinski NR, Teufel LW. 1987. Influence of geologic discontinuities on hydraulic fracture propagation. *J. Pet. Technol.* 39:209–20
69. Smart KJ, Ofoegbu GI, Morris AP, McGinnis RN, Ferrill DA. 2014. Geomechanical modeling of hydraulic fracturing: why mechanical stratigraphy, stress state, and pre-existing structure matter. *AAPG Bull.* 98:2237–61
70. Rassenfoss S. 2015. What do fractures look like? A picture says a lot, even when it is wrong. *J. Pet. Technol.* 67(5):60–68
71. Fisher K, Warpinski N. 2012. Hydraulic-fracture-height growth: real data. *SPE Prod. Oper.* 27:8–19
72. Yew CH, Weng X. 2014. *Mechanics of Hydraulic Fracturing*. Houston: Gulf Prof. Publ. 2nd ed.
73. Smith MB, Shylapobersky JW. 1999. Basics of hydraulic fracturing. In *Reservoir Stimulation*, ed. MJ Economides, KG Nolte, pp. 5.1–5.28. New York: John Wiley & Sons
74. Cipolla CL, Warpinski NR, Mayerhofer MJ, Lolon E, Vincent MC. 2008. *The relationship between fracture complexity, reservoir properties, and fracture treatment design*. Presented at SPE Annu. Tech. Conf. Exhib. Sept. 21–24, Denver, CO
75. Warpinski NR, Wolhart SL, Wright CA. 2001. *Analysis and prediction of microseismicity induced by hydraulic fracturing*. Presented at SPE Annu. Tech. Conf. Exhib., Sept. 30–Oct. 3, New Orleans, LA
76. Adachi J, Siebrits E, Peirce A, Desroches J. 2007. Computer simulations of hydraulic fractures. *Int. J. Rock Mech. Min. Sci.* 44:739–57
77. Perkins TK, Kern LR. 1961. Widths of hydraulic fractures. *J. Pet. Technol.* 13:937–49
78. Nordgren RP. 1972. Propagation of a vertical hydraulic fracture. *Soc. Pet. Eng. J.* 12:306–14
79. Khristianovich SA, Zheltov YP. 1955. *Formation of vertical fractures by means of highly viscous liquids.* Presented at Fourth World Pet. Congr., June 6–15, Rome, Italy
80. Geertsma J, de Klerk F. 1969. A rapid method of predicting width and extent of hydraulically induced fractures. *J. Pet. Technol.* 21:1571–81
81. Abé H, Mura T, Keer LM. 1976. Growth rate of a penny-shaped crack in hydraulic fracturing of rocks. *J. Geophys. Res.* 81:5335–40
82. England AH, Green AE. 1963. Some two-dimensional punch and crack problems in classical elasticity. *Math. Proc. Camb. Philos. Soc.* 59:489–500
83. Geertsma J. 1989. Two-dimensional fracture-propagation models. In *Recent Advances in Hydraulic Fracturing*, Vol. 12, *Henry L. Dougherty Series*, ed. JL Gidley, SA Holditch, DE Nierode, RW Veatch Jr., pp. 81–94. Richardson, TX: Soc. Pet. Eng.
84. Barenblatt GI. 1959. The formation of equilibrium cracks during brittle fracture. General ideas and hypotheses. Axially-symmetric cracks. *J. Appl. Math. Mech.* 23:622–36
85. Rice J. 1968. Mathematical analysis in the mechanics of fracture. In *Fracture: An Advanced Treatise*, Vol. 2, ed. H Liebowitz, pp. 191–311. Cambridge: Academic
86. Howard GC, Fast CR. 1957. *Optimum fluid characteristics for fracture extension*. Presented at Drill. Prod. Pract., Jan. 1, New York
87. Madyarova MV. 2003. *Fluid-driven penny-shaped fracture in permeable rock*. Master's Thesis, Univ. Minn., Minneapolis
88. Carter BJ, Desroches J, Ingraffea AR, Wawrzynek PA. 2000. Simulating 3D hydraulic fracturing. In *Modeling in Geomechanics*, ed. M Zaman, G Gioda, JR Booker, pp. 525–57. Hoboken, NJ: John Wiley & Sons

89. Spence DA, Sharp PW. 1985. Self-similar solutions for elastohydrodynamic cavity flow. *Proc. R. Soc. Lond. A Math. Phys. Eng. Sci.* 400:289–313
90. Spence DA, Turcotte DL. 1985. Magma-driven propagation of cracks. *J. Geophys. Res.* 90:575–80
91. Spence DA, Sharp PW, Turcotte DL. 1987. Buoyancy-driven crack propagation: a mechanism for magma migration. *J. Fluid Mech.* 174:135–53
92. Lister JR. 1990. Buoyancy-driven fluid fracture: the effects of material toughness and of low-viscosity precursors. *J. Fluid Mech.* 210:263–80
93. Desroches J, Detournay E, Lenoach B, Papanastasiou P, Pearson JRA, et al. 1994. The crack tip region in hydraulic fracturing. *Proc. R. Soc. Lond. A Math. Phys. Eng. Sci.* 447:39–48
94. Garagash D, Detournay E. 2000. The tip region of a fluid-driven fracture in an elastic medium. *J. Appl. Mech.* 67:183–92
95. Detournay E. 2004. Propagation regimes of fluid-driven fractures in impermeable rocks. *Int. J. Geomech.* 4:35–45
96. Garagash DI. 2009. Scaling of physical processes in fluid-driven fracture: perspective from the tip. In *IUTAM Symposium on Scaling in Solid Mechanics*, Vol. 10, *Iutam Bookseries*, ed. F Borodich, pp. 91–100. Dordrecht, Neth.: Springer
97. Garagash DI, Detournay E, Adachi JI. 2011. Multiscale tip asymptotics in hydraulic fracture with leak-off. *J. Fluid Mech.* 669:260–97
98. Lenoach B. 1995. The crack tip solution for hydraulic fracturing in a permeable solid. *J. Mech. Phys. Solids* 43:1025–43
99. Bunger AP, Detournay E, Garagash Dmitry I. 2005. Toughness-dominated hydraulic fracture with leak-off. *Int. J. Fract.* 134:175–90
100. Detournay E. 2016. Mechanics of hydraulic fractures. *Annu. Rev. Fluid Mech.* 48:311–39
101. Brown SR. 1987. Fluid flow through rock joints: the effect of surface roughness. *J. Geophys. Res.* 92:1337–47
102. Mewis J, Wagner NJ. 2013. *Colloidal Suspension Rheology*. Cambridge: Cambridge Univ. Press
103. Guazzelli E, Morris JF. 2012. *A Physical Introduction to Suspension Dynamics*. Cambridge: Cambridge Univ. Press
104. Khilar KC, Fogler HS. 1998. *Migration of Fines in Porous Media*. Dordrecht, Neth.: Kluwer
105. Ely JW. 1989. Fracturing fluids and additives. In *Recent Advances in Hydraulic Fracturing*, ed. JL Gidley, SA Holditch, DE Nierode, W Veatch Jr., pp. 131–46. Richardson, TX: Soc. Pet. Eng.
106. Montgomery C. 2013. *Fracturing fluids.* Presented at ISRM Int. Conf. Eff. Sustain. Hydraul. Fract., May 20–22, Brisbane, Aust.
107. Bird RB, Armstrong RC, Hassager O. 1987. *Dynamics of Polymeric Liquids*, Vol. 1: *Fluid Mechanics*. Hoboken, NJ: Wiley Intersci.
108. Larson RG. 1998. *The Structure and Rheology of Complex Fluids*. Oxford: Oxford Univ. Press
109. Joseph DD. 1990. *Fluid Dynamics of Viscoelastic Liquids*. New York: Springer
110. Ho BP, Leal LG. 1976. Migration of rigid spheres in a two-dimensional unidirectional shear flow of a second-order fluid. *J. Fluid Mech.* 76:783–99
111. Leshansky AM, Bransky A, Korin N, Dinnar U. 2007. Tunable nonlinear viscoelastic "focusing" in a microfluid device. *Phys. Rev. Lett.* 98:234501
112. Larson RG, Shaqfeh ESG, Muller SJ. 1990. A purely elastic instability in Taylor-Couette flow. *J. Fluid Mech.* 218:573–600
113. McKinley GH, Pakdel P, Oztekin A. 1996. Geometric and rheological scaling of purely elastic flow instabilities. *J. Non-Newton. Fluid Mech.* 67:19–48
114. Barati R, Liang JT. 2014. A review of fracturing fluid systems used for hydraulic fracturing of oil and gas wells. *J. Appl. Polym. Sci.* 131:40735
115. Gulbis J, Hodge RM. 1999. Fracturing fluid chemistry and proppants. In *Reservoir Stimulation*, ed. MJ Economides, KG Nolte, pp. 7.1–7.23. Hoboken, NJ: John Wiley & Sons
116. Clark AH, Ross-Murphy SB. 1987. Structural and mechanical properties of biopolymer gels. In *Biopolymers*, ed. H Benoit, H-J Cantow, G Dall'Asta, K Dusek, H Fujita, et al., pp. 57–192. Berlin: Springer
117. Mathur NK. 2012. *Industrial Galactomannan Polysaccharides*. Boca Raton, FL: CRC Press

118. Wientjes RHW, Duits MHG, Jongschaap RJJ, Mellema J. 2000. Linear rheology of guar gum solutions. *Macromolecules* 33:9594–605
119. Kesavan S, Prud'homme RK. 1992. Rheology of guar and (hydroxypropyl) guar crosslinked by borate. *Macromolecules* 25:2026–32
120. Pezron E, Ricard A, Lafuma F, Audebert R. 1988. Reversible gel formation induced by ion complexation. 1. Borax–galactomannan interactions. *Macromolecules* 21:1121–25
121. Bishop M, Shahid N, Yang J, Barron AR. 2004. Determination of the mode and efficacy of the cross-linking of guar by borate using MAS ^{11}B NMR of borate cross-linked guar in combination with solution ^{11}B NMR of model systems. *Dalton Trans.* 2004:2621–34
122. Hu YT. 2014. Mechanism of shear thickening in transient guar network. *J. Rheol.* 58:1789–807
123. Kramer J, Prud'homme RK, Wiltzius P, Knoll S. 1988. Comparison of galactomannan crosslinking with organotitanates and borates. *Colloid Polym. Sci.* 266:145–55
124. Parris MD, MacKay BA, Rathke JW, Klingler RJ, Gerald RE II. 2008. Influence of pressure on boron cross-linked polymer gels. *Macromolecules* 41:8181–86
125. Vega-Cantu YI, Hauge RH, Norman LR, Powell RJ, Billups WE. 2006. Effect of magnesium and iron on the hydration and hydrolysis of guar gum. *Biomacromolecules* 7:441–45
126. Tayal A, Pai VB, Khan SA. 1999. Rheology and microstructural changes during enzymatic degradation of a guar–borax hydrogel. *Macromolecules* 32:5567–74
127. Dreiss CA. 2007. Wormlike micelles: Where do we stand? Recent developments, linear rheology and scattering techniques. *Soft Matter* 3:956–70
128. Khan SA, Schnepper CA, Armstrong RC. 1988. Foam rheology: III. Measurement of shear flow properties. *J. Rheol.* 32:69–92
129. Yoshimura A, Prud'homme RK. 1988. Wall slip corrections for Couette and parallel disk viscometers. *J. Rheol.* 32:53–67
130. Hurst RE. 1972. *Gas frac—a new stimulation technique using liquid gases.* Presented at Soc. Pet. Eng. Rocky Mountain Reg. Meet., April 10–12, Denver, CO
131. Soni TM. 2014. *LPG-based fracturing: an alternate fracturing technique in shale reservoirs*. Presented at IADC/SPE Asia Pac. Drill. Technol. Conf., Aug. 25–27, Bangkok, Thail.
132. Palisch TT, Vincent MC, Handren PJ. 2008. *Slickwater fracturing: food for thought*. Presented at Soc. Pet. Eng. Annu. Tech. Conf. Exhib., Sept. 21–24, Denver, CO
133. White CM, Mungal MG. 2008. Mechanics and prediction of turbulent drag reduction with polymer additives. *Annu. Rev. Fluid Mech.* 40:235–56
134. Sharma MM, Gadde PB, Sullivan R, Sigal R, Fielder R, et al. 2005. Slick-water and hybrid fracturing treatments: lessons learned. *J. Pet. Technol.* 57:38–40
135. Bivins CH, Boney C, Fredd C, Lassek J, Sullivan P, et al. 2005. New fibers for hydraulic fracturing. *Oilfield Rev.* Summer:34–43
136. Warpinski NR. 2009. *Stress amplification and arch dimensions in proppant beds deposited by waterfracs*. Presented at SPE Hydraul. Fract. Technol. Conf., Jan. 19–21, The Woodlands, TX
137. Larson RG. 1988. *Constitutive Equations for Polymer Melts and Solutions*. London: Butterworths
138. Anna SL, McKinley GH, Nguyen DA, Sridhar T, Muller SJ, et al. 2001. An interlaboratory comparison of measurements from filament-stretching rheometers using common test fluids. *J. Rheol.* 45:83–114
139. McKinley GH, Sridhar T. 2002. Filament-stretching rheometry of complex fluids. *Annu. Rev. Fluid Mech.* 34:375–415
140. Rodd LE, Scott TP, Cooper-White JJ, McKinley GH. 2005. Capillary breakup rheometry of low-viscosity elastic fluids. *Appl. Rheol.* 15:12–27
141. Macosko CW. 1994. *Rheology: Principles, Measurements, and Applications*. Weinheim, Ger.: Wiley-VCH
142. Manneville S. 2008. Recent experimental probes of shear banding. *Rheol. Acta* 47:301–18
143. Larson RG. 1992. Instabilities in viscoelastic flows. *Rheol. Acta* 31:213–63
144. Eberle APR, Baird DG, Wapperom P. 2008. Rheology of non-Newtonian fluids containing glass fibers: a review of experimental literature. *Ind. Eng. Chem. Res.* 47:3470–88
145. Prud'homme RK, Ellis S, Constien VG, Knoll S. 1988. *Reproducible rheological measurements on crosslinked fracturing fluids.* Presented at SPE Annu. Tech. Conf. Exhib., Oct. 2–5, Houston, TX

146. Walker RNJ, Hunter JL, Brake AC, Fagin PA, Steinsberger N. 1998. *Proppants, we still don't need no proppants—a perspective of several operators.* Presented at SPE Annu. Tech. Conf. Exhib., Sept. 27–30, New Orleans, LA
147. Montgomery CT, Smith MB. 2010. Hydraulic fracturing: history of an enduring technology. *J. Pet. Technol.* 62:26–40
148. Stickel JJ, Powell RL. 2005. Fluid mechanics and rheology of dense suspensions. *Annu. Rev. Fluid Mech.* 37:129–49
149. Farris RJ. 1968. Prediction of the viscosity of multimodal suspensions from unimodal viscosity data. *Trans. Soc. Rheol.* 12:281–301
150. Chang C, Powell RL. 1994. Effect of particle size distribution on the rheology of concentrated bimodal suspensions. *J. Rheol.* 38:85–98
151. Panga MKR, Bedel JP, Chen Y. 2014. *High solids content slurries, systems and methods.* US Patent No. 8,916,506
152. Jeffery GB. 1922. The motion of ellipsoidal particles immersed in a viscous fluid. *Proc. R. Soc. Lond. A Papers Math. Phys. Character* 102:161–79
153. Petrie CJS. 1999. The rheology of fibre suspensions. *J. Non-Newton. Fluid Mech.* 87:369–402
154. Djalili-Moghaddam M, Toll S. 2006. Fibre suspension rheology: effect of concentration, aspect ratio and fiber size. *Rheol. Acta* 45:315–20
155. Chaouche M, Koch DL. 2001. Rheology of non-Brownian rigid fiber suspensions with adhesive contacts. *J. Rheol.* 45:369–82
156. Garboczi EJ, Snyder KA, Douglas JF, Thorpe MF. 1995. Geometrical percolation threshold of overlapping ellipsoids. *Phys. Rev. E Stat. Nonlinear Soft Matter Phys.* 52:819–28
157. Barnes HA. 1989. Shear-thickening ("dilatancy") in suspensions of nonaggregating solid particles dispersed in Newtonian liquids. *J. Rheol.* 33:329–66
158. Denn MM, Morris JF. 2014. Rheology of non-Brownian suspensions. *Annu. Rev. Chem. Biomol. Eng.* 5:203–28
159. Barnes HA. 2003. A review on the rheology of filled viscoelastic systems. *Rheol. Rev.* 2003:1–36
160. Ohl N, Gleissle W. 1993. The characterization of the steady-state shear and normal stress functions of highly concentrated suspensions formulated with viscoelastic liquids. *J. Rheol.* 37:381–406
161. Mall-Gleissle SE, Gleissle W, McKinley GH, Buggisch H. 2002. The normal stress behavior of suspensions with viscoelastic matrix fluids. *Rheol. Acta* 42:61–76
162. Dagois-Bohy S, Hormozi S, Guazzelli E, Pouliquen O. 2015. Rheology of dense suspensions of non-colloidal spheres in yield-stress fluids. *J. Fluid Mech.* 776:R2
163. Nolte KG. 1988. *Fluid flow considerations in hydraulic fracturing*. Presented at SPE East. Reg. Meet., Nov. 1–4, Charleston, WV
164. Van der Vlis AC, Haafkens R, Schipper BA, Visser W. 1975. *Criteria for proppant placement and fracture conductivity*. Presented at Fall Meet. Soc. Pet. Eng. AIME, Sept. 28–Oct. 1, Dallas, TX
165. Segré G, Silberberg A. 1962. Behaviour of macroscopic rigid spheres in Poiseuille flow part 1. Determination of local concentration by statistical analysis of particle passages through crossed light beams. *J. Fluid Mech.* 14:115–35
166. Segré G, Silberberg A. 1962. Behaviour of macroscopic rigid spheres in Poiseuille flow part 2. Experimental results and interpretation. *J. Fluid Mech.* 14:136–57
167. Ho BP, Leal LG. 1974. Inertial migration of rigid spheres in two-dimensional unidirectional flows. *J. Fluid Mech.* 65:365–400
168. Schonberg JA, Hinch EJ. 1989. Inertial migration of a sphere in Poiseuille flow. *J. Fluid Mech.* 203:517–24
169. Matas JP, Morris JF, Guazzelli E. 2004. Inertial migration of rigid spherical particles in Poiseuille flow. *J. Fluid Mech.* 515:171–95
170. Asmolov ES. 1999. The inertial lift on a spherical particle in a plane Poiseuille flow at large channel Reynolds number. *J. Fluid Mech.* 381:63–87
171. Gadala-Maria F, Acrivos A. 1980. Shear-induced structure in a concentrated suspension of solid spheres. *J. Rheol.* 24:799–814
172. Leighton D, Acrivos A. 1987. The shear-induced migration of particles in concentrated suspensions. *J. Fluid Mech.* 181:415–39

173. Koh CJ, Hookham P, Leal LG. 1994. Experimental investigation of concentrated suspension flows in a rectangular channel. *J. Fluid Mech.* 266:1–32
174. Lyon MK, Leal LG. 1998. An experimental study of the motion of concentrated suspensions in two-dimensional channel flow. Part 1. Monodisperse systems. *J. Fluid Mech.* 363:25–56
175. Oh S, Song Yq, Garagash DI, Lecampion B, Desroches J. 2015. Pressure-driven suspension flow near jamming. *Phys. Rev. Lett.* 114:088301
176. Phillips RJ, Armstrong RC, Brown RA, Graham AL, Abbott JR. 1992. A constitutive equation for concentrated suspensions that accounts for shear-induced particle migration. *Phys. Fluids A* 4:30–40
177. Mills P, Snabre P. 1995. Rheology and structure of concentrated suspensions of hard spheres. Shear induced particle migration. *J. Phys. II* 5:1597–608
178. Lecampion B, Garagash D. 2014. Confined flow of suspensions modelled by a frictional rheology. *J. Fluid Mech.* 759:197–235
179. Dontsov EV, Peirce AP. 2014. Slurry flow, gravitational settling and a proppant transport model for hydraulic fractures. *J. Fluid Mech.* 760:567–90
180. Boyer B, Guazelli E, Pouliquen O. 2011. Unifying suspension and granular rheology. *Phys. Rev. Lett.* 107:188301
181. Tehrani MA. 1996. An experimental study of particle migration in pipe flow of viscoelastic fluids. *J. Rheol.* 40:1057–77
182. Feng J, Joseph DD. 1996. The motion of solid particles suspended in viscoelastic liquids under torsional shear. *J. Fluid Mech.* 324:199–222
183. Lim EJ, Ober TJ, Edd JF, Desai SP, Neal D, et al. 2014. Inertio-elastic focusing of bioparticles in microchannels at ultra-high throughput. *Nat. Commun.* 5:1460
184. Iso Y, Koch DL, Cohen C. 1996. Orientation in simple shear flow of semi-dilute fiber suspensions 1. Weakly elastic fluids. *J. Non-Newton. Fluid Mech.* 62:115–34
185. Iso Y, Cohen C, Koch DL. 1996. Orientation in simple shear flow of semi-dilute fiber suspensions 2. Highly elastic fluids. *J. Non-Newton. Fluid Mech.* 62:135–53
186. Snijkers F, Pasquino R, Vermant J. 2013. Hydrodynamic interactions between two equally sized spheres in viscoelastic fluids in shear flow. *Langmuir* 29:5701–13
187. Joseph DD, Feng J. 1996. A note on the forces that move particles in a second-order fluid. *J. Non-Newton. Fluid Mech.* 64:299–302
188. Daneshy A. 1989. Proppant transport. In *Recent Advances in Hydraulic Fracturing*, pp. 210–22. Richardson, TX: Soc. Pet. Eng.
189. Kern LR, Perkins TK, Wyant RE. 1959. The mechanics of sand movement in fracturing. *J. Pet. Technol.* 11:55–57
190. McLennan JD, Green SJ, Bai M. 2008. *Proppant placement during tight gas shale stimulation: literature review and speculation.* Presented at 42nd US Rock Mech. Symp., 2nd US-Canada Rock Mech. Symp., June 29–July 2, San Francisco, CA
191. Miller KC, McCave IN, Komar PD. 1977. Threshold of sediment motion under unidirectional currents. *Sedimentology* 24:507–27
192. Patankar NA, Joseph DD, Wang J, Barree RD, Conway M, Asadi M. 2002. Power law correlations for sediment transport in pressure driven channel flows. *Int. J. Multiph. Flow* 28:1269–92
193. Wang J, Joseph DD, Patankar NA, Conway M, Barree RD. 2003. Bi-power law correlations for sediment transport in pressure driven channel flows. *Int. J. Multiph. Flow* 29:475–94
194. Richardson JF, Zaki WN. 1954. The sedimentation of a suspension of uniform spheres under conditions of viscous flow. *Chem. Eng. Sci.* 8:65–73
195. Richardson JF, Zaki WN. 1954. Sedimentation and fluidisation: part I. *Trans. Inst. Chem. Eng.* 32:S82–S100
196. Chang C, Powell RL. 2002. Hydrodynamic transport properties of concentrated suspensions. *Am. Inst. Chem. Eng. J.* 48:2475–80
197. Roodhart LP. 1985. *Proppant settling in non-Newtonian fracturing fluids.* Presented at SPE/DOE 1985 Low Permeability Gas Reserv. Symp., March 19–22, Denver, CO
198. Acharya AR. 1988. Viscoelasticity of crosslinked fracturing fluids and proppant transport. *SPE Prod. Eng.* 3:483–88

199. Novotny EJ. 1977. *Proppant transport.* Presented at SPE Annu. Fall Tech. Conf. Exhib., Oct. 9–12, Denver, CO
200. McMechan DE, Shah SN. 1991. Static proppant-settling characteristics of non-Newtonian fracturing fluids in a large-scale test model. *SPE Prod. Eng.* 6:305–12
201. Padhy S, Shaqfeh ESG, Iaccarino G, Morris JF, Tonmukayakul N. 2013. Simulations of a sphere sedimenting in a viscoelastic fluid with cross shear flow. *J. Non-Newton. Fluid Mech.* 197:48–60
202. Tonmukayakul N, Bryant JE, Talbot MS, Morris JF. 2008. *Dynamic and steady shear properties of reversibly cross-linked guar solutions and their effects on particle settling behavior.* Presented at XVth Int. Congr. Rheol., Soc. Rheol. 80th Annu. Meet., Aug. 3–8, Monterey, CA
203. Won D, Kim C. 2004. Alignment and aggregation of spherical particles in viscoelastic fluid under shear flow. *J. Non-Newton. Fluid Mech.* 117:141–46
204. Mora S, Talini L, Allain C. 2005. Structuring sedimentation in a shear-thinning fluid. *Phys. Rev. Lett.* 95:088301
205. van den Brule BHAA, Gheissary G. 1993. Effects of fluid elasticity on the static and dynamic settling of a spherical particle. *J. Non-Newton. Fluid Mech.* 49:123–32
206. Gheissary G, van den Brule BHAA. 1996. Unexpected phenomena observed in particle settling in non-Newtonian media. *J. Non-Newton. Fluid Mech.* 67:1–18
207. Hu YT, Chung H, Maxey J. 2015. *What is more important for proppant transport, viscosity or elasticity?* Presented at SPE Hydraul. Fract. Technol. Conf., Feb. 3–5, The Woodlands, TX
208. Hu YT, Larsen T, Martysevich V. 2015. *Study of proppant suspending using multipass slot flow apparatus*. Presented at SPE Prod. Oper. Symp., March 1–5, Oklahoma City, OK
209. Hu YT, Kishore T, Maxey J, Loveless D. 2015. *Effects of crosslinking chemistry on proppant suspension in guar networks.* Presented at SPE Int. Symp. Oilfield Chem., April 13–15, The Woodlands, TX
210. Housiadas KD, Tanner RI. 2012. The drag of a freely sedimenting sphere in a sheared weakly viscoelastic fluid. *J. Non-Newton. Fluid Mech.* 183–84:52–56
211. Tanner RI, Housiadas KD, Qi F. 2014. Mechanism of drag increase on spheres in viscoelastic cross-shear flow. *J. Non-Newton. Fluid Mech.* 203:51–53
212. Padhy S, Rodriguez M, Shaqfeh ESG, Iaccarino G, Morris JF, Tonmukayakul N. 2013. The effect of shear thinning and walls on the sedimentation of a sphere in an elastic fluid under orthogonal shear. *J. Non-Newton. Fluid Mech.* 201:120–29
213. Chekhonin E, Levonyan K. 2012. Hydraulic fracture propagation in highly permeable formations, with applications to tip screenout. *Int. J. Rock Mech. Min. Sci.* 50:19–28
214. Dontsov EV, Peirce AP. 2014. *The effect of proppant size on hydraulic fracturing by a slurry.* Presented at 48th US Rock Mech./Geomech. Symp., June 1–4, Minneapolis, MN
215. Dontsov EV, Peirce AP. 2015. Proppant transport in hydraulic fracturing: crack tip screen-out in KGD and P3D models. *Int. J. Solids Struct.* 63:206–18
216. To K, Lai PK, Pak HK. 2001. Jamming of granular flow in a two-dimensional hopper. *Phys. Rev. Lett.* 86:71
217. Roussel N, Nguyen TLH, Coussot P. 2007. General probabilistic approach to the filtration process. *Phys. Rev. Lett.* 98:114502
218. Mari R, Seto R, Morris JF, Denn MM. 2014. Shear thickening, frictionless and frictional rheologies in non-Brownian suspensions. *J. Rheol.* 58:1693–724
219. Potapenko DI, Tinkham SK, Lecerf B, Fredd CN, Samuelson ML, et al. 2009. *Barnett shale infrastructure stimulations using a novel diversion technique*. Presented at SPE Hydraul. Fract. Technol. Conf., Jan. 19–21, The Woodlands, TX
220. Kaageson-Loe N, Sanders MW, Growcock F, Taugh LK, Hosrud P, et al. 2009. Particulate-based loss-prevention material—the secrets of fracture sealing revealed. *SPE Drill. Complet.* 24(4):581–89
221. Advani SH, Torok JS, Lee JK, Choudhry S. 1987. Explicit time-dependent solutions and numerical evaluations for penny-shaped hydraulic fracture models. *J. Geophys. Res.* 91(B8):8049–55